SIAM J. SCI. COMPUT.
Vol. 20, No. 5, pp. 1875–1904

THE FINITE ELEMENT APPROXIMATION OF SEMILINEAR ELLIPTIC PARTIAL DIFFERENTIAL EQUATIONS WITH CRITICAL EXPONENTS IN THE CUBE*

C. J. BUDD†, A. R. HUMPHRIES‡, AND A. J. WATHEN§

Abstract. We consider the finite element solution of the parameterized semilinear elliptic equation $\Delta u + \lambda u + u^5 = 0, u > 0$, where u is defined in the unit cube and is 0 on the boundary of the cube. This equation is important in analysis, and it is known that there is a value $\lambda_0 > 0$ such that no solutions exist for $\lambda < \lambda_0$. By solving a related linear equation we obtain an upper bound for λ_0 which is also conjectured to be an estimate for its value. We then present results on computations on the full nonlinear problem. Using formal asymptotic methods we derive an approximate description of u which is supported by the numerical calculations. The asymptotic methods also give sharp estimates both for the error in the finite element solution when $\lambda > \lambda_0$ and for the form of the spurious numerical solutions which are known to exist when $\lambda < \lambda_0$. These estimates are then used to post-process the numerical results to obtain a sharp estimate for λ_0 which agrees with the conjectured value.

Key words. semilinear elliptic partial differential equations, finite element method, critical Sobolev exponent, spurious solutions, matched asymptotic expansion

AMS subject classifications. 35J60, 65N30, 46E35, 65N12, 41A60

PII. S1064827596312134

1. Introduction.

1.1. Preliminaries. An important class of parameterized semilinear elliptic partial differential equations with solutions which develop isolated singularities as the parameter varies is given by the system

$$\left.\begin{array}{ll} \Delta u + \lambda u + u^5 = 0 & \text{on } \Omega \subset \mathbb{R}^3, \\ u > 0 & \text{in } \Omega, \\ u = 0 & \text{on } \partial\Omega, \end{array}\right\} \tag{1.1}$$

where Ω is a bounded domain in $\mathbb{R}^3$. For this problem there exist domains Ω and a parameter $\lambda_0 > 0$ such that $\|u\|_\infty \to \infty$ as $\lambda \to \lambda_0$ with no (positive) solution existing when $\lambda < \lambda_0$. Our studies focus on the finite element approximation of u close to this singularity, calculating λ_0 accurately and deriving sharp error estimates which also describe the behavior of the numerical solutions when $\lambda < \lambda_0$.

The model problem (1.1) was introduced by Brezis and Nirenberg in the seminal paper [2] as a special case of the more general problem

$$\left.\begin{array}{ll} \Delta u + f(u;\lambda) = 0 & \text{on } \Omega \subset \mathbb{R}^n, \quad n \geqslant 3, \\ u > 0 & \text{in } \Omega, \\ u = 0 & \text{on } \partial\Omega, \end{array}\right\} \tag{1.2}$$

*Received by the editors November 18, 1996; accepted for publication (in revised form) October 15, 1997; published electronically May 18, 1999. This work was supported by the Engineering and Physical Sciences Research Council, UK, through grants GR/H63456 and GR/J75258.
http://www.siam.org/journals/sisc/20-5/31213.html
†School of Mathematics, University of Bath, Claverton Down, Bath BA2 7AY, UK (cjb@maths.bath.ac.uk).
‡Centre for Mathematical Analysis and its Applications, School of Mathematical Sciences, University of Sussex, Brighton, BN1 9QH, UK (a.r.humphries@susx.ac.uk).
§Oxford University Computing Laboratory, Wolfson Building, Parks Road, Oxford OX1 3QD, UK (wathen@comlab.ox.ac.uk).

where the function $f(u;\lambda)$ has the property that as $u \to \infty$ there exists a strictly positive constant C such that

$$f(u;\lambda)u^{-p_c} \to C, \quad \text{where } p_c \equiv \frac{n+2}{n-2}, \quad n \geqslant 3. \tag{1.3}$$

The value p_c is called the critical Sobolev exponent for $\mathbb{R}^n$, $n \geqslant 3$, and f is said to grow at a critical rate. The most subtle behavior is observed in the case of $n = 3$ and $p_c = 5$, which is that studied in this paper.

The study of (1.1) and (1.2) was originally motivated by the *Yamabé problem* of constructing a manifold of a given curvature, which requires the solution of a critical problem related to (1.1) and (1.2) on a Riemannian manifold; it also has applications in the study of stellar structure. However, the challenges posed by (1.1) and (1.2) are such that these equations have been studied as problems in analysis and have provided a rich source of open and fascinating problems. The reason for this richness is that if the function f grows more slowly than the critical rate, then variational techniques may be used in the analysis of (1.2); however, these techniques break down for critically growing nonlinearities. This leads to delicate questions concerning the existence (in particular the value of λ_0 at which solutions cease to exist), the uniqueness, and the regularity of the solutions. The analytic investigations of the solution branch (λ, u) of (1.1) have mostly concentrated upon radially symmetric solutions in the sphere and these investigations have led to many conjectures about the behavior in more general domains. The first purpose of this paper is to apply the finite element method to perform a numerical study of the branch (λ, U_h) of discrete solutions of a weak form of (1.1) when Ω is the unit cube. For this investigation we consider for simplicity piecewise trilinear functions defined on a uniform mesh of element size h. Experiments with higher order elements on symmetric domains [5] have shown that these do not offer any significant advantage over linear elements for the rejection of spurious solutions. Uniformity of the mesh allows the use of an effective extrapolation procedure for post-processing the results. We give numerical evidence to support some outstanding conjectures on the value of λ_0, the uniqueness of the solution, and the behavior of the solution as it becomes more singular in the limit of $\lambda \to \lambda_0$.

Because the finite element method is based upon variational ideas, it inherits many of the interesting structures of the continuous problem related to the breakdown of the variational method. Consequently, its application to solving (1.1) is delicate, and we need to introduce several new ideas to determine the solution accurately and to obtain good error estimates for $\|U_h - u\|_\infty$. Difficulties arise for two reasons. First, both u and Δu become unbounded as λ approaches λ_0. Second, the differential operator L_λ derived by linearizing (1.1) about the solution and defined by

$$L_\lambda \varphi = \Delta\varphi + \lambda\varphi + 5u^4\varphi, \quad \varphi|_{\partial\Omega} = 0, \tag{1.4}$$

is known to have an inverse which itself becomes unbounded in the L_∞ operator norm as $\lambda \to \lambda_0$ [4]. Estimates of the error $\|U_h - u\|_\infty$ in the solution of (1.1) are presented in [9], [8]. These are proportional to the product of $\|\Delta u\|_\infty$ and $\|L^{-1}\|_\infty$ and consequently are very large as $\lambda \to \lambda_0^+$. Furthermore, variational arguments prove that spurious numerical solutions of (1.1) exist when $\lambda \leqslant \lambda_0$. Unlike convergent solutions, the maximum norm of the spurious solutions grows without bound as $h \to 0$. However, we show that this growth is slow, being proportional to $h^{-1/4}$. The spurious solutions lie on the same continuous solution branch as those which converge to u

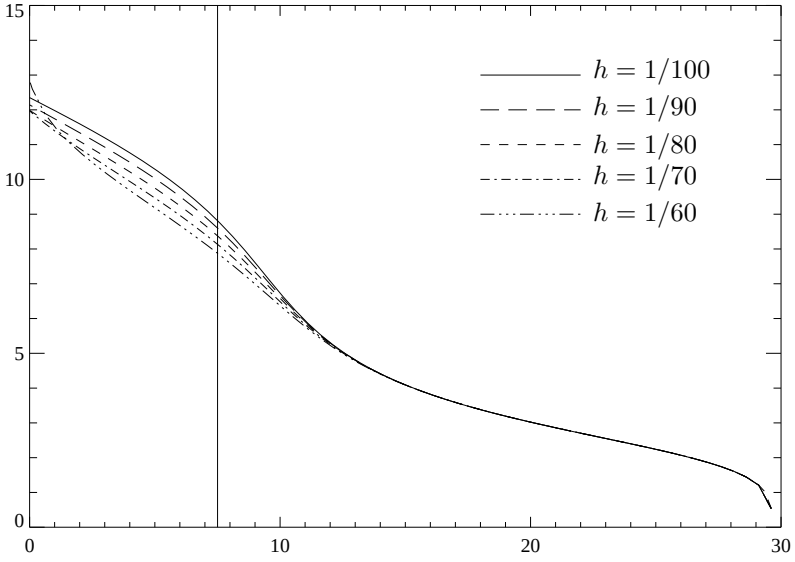

FIG. 1.1. *Graph of* $\|U_h\|_\infty$ *against* λ, *for grids varying between* $h = 1/60$ *and* $h = 1/100$, *with* λ_0 *indicated by the vertical line.*

under mesh refinement and are almost indistinguishable from them if λ_0 is unknown. Consequently, the range of existence of the true solutions is hard to determine.

In Figure 1.1 we present a graph of the infinity norm of the discrete solution U_h as a function of λ and also indicate a value of $\lambda_0 = 7.5045$ which is conjectured from further computations in this paper. This graph was obtained for a solution of (1.1) on the unit cube $0 \leqslant x, y, z \leqslant 1$ using the finite element method with piecewise trilinear basis functions defined over cubes of side $h = 1/60, \ldots, 1/100$. Observe that each of the curves looks smooth with no significant hint of singular behavior occurring close to λ_0.

In Figure 1.2 we present a cross section of the resulting solution taken in the plane $z = 1/2$ with $h = 1/100$ for $\lambda =$ (a) 20, (b) 15, (c) 7.5045, (d) 0. In this graph figures (a) and (b) are approximations to true solutions, (d) is certainly spurious, and further computations strongly imply that (c) is also spurious. From these figures we observe that each of these figures exhibits a peak forming in the center of the cube which grows as λ is reduced. Although the peak in (c) and (d) is higher than those in (a) and (b), its appearance does not appear to be significantly different (i.e., it appears well resolved by the mesh) and it is very hard a priori to distinguish from numerical evidence alone between the true and spurious solutions.

As the singularity forms it is computationally impossible to use a fine enough uniform mesh to resolve its structure, and indeed the employment of a fixed mesh ultimately leads to the spurious solutions. This suggests that an adaptive approach which places a higher density of mesh points close to the singularity should be taken. Such methods are hard to implement in three dimensions; moreover, they typically make use of an a priori or a posteriori estimate of the local truncation and these estimates are not sharp for (1.1) due to the unboundedness of $\|L_\lambda^{-1}\|_\infty$. Some preliminary computations of radially symmetric solutions of (1.1) reported in [6] demonstrate that

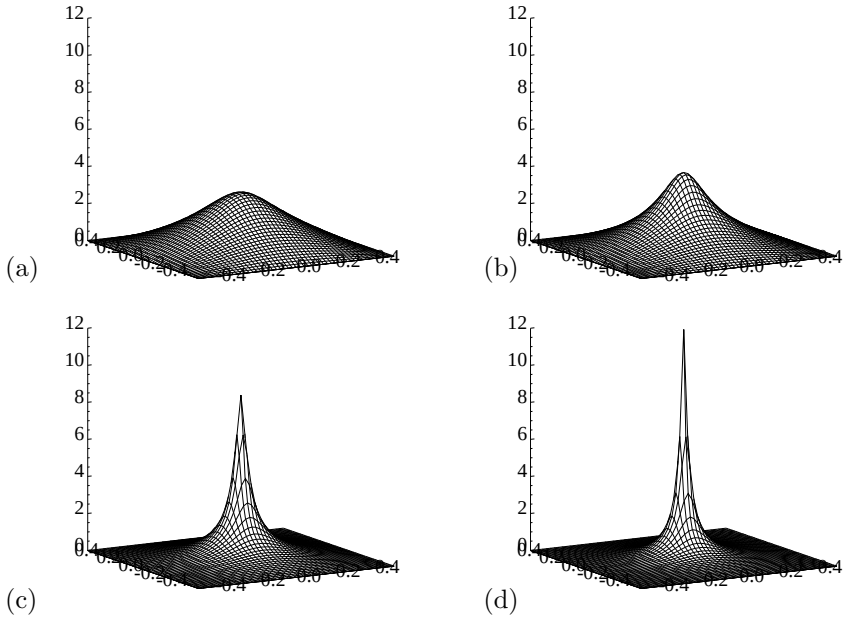

FIG. 1.2. *Cross section of the numerical solution U_h through center of cube with $h = 1/100$ and* (a) $\lambda = 20$, (b) $\lambda = 15$, (c) $\lambda = \lambda_{**} = 7.5045$, (d) $\lambda = 0$.

adaptive methods based upon local truncation or a posteriori error estimates are not particularly accurate and still admit spurious solutions. As a consequence, we adopt a different approach here by looking at the solution on a uniform mesh and use formal asymptotic methods, scaling arguments, and an approximation result (in Lemma 6.1) to obtain sharp estimates of both the convergent and the spurious solutions. By using sufficiently fine meshes these estimates are descriptive and can be used to post-process the numerical solution to give a much more accurate solution of (1.1) and an estimate of λ_0. We show that if λ is close to but greater than λ_0, then there is a constant C such that if h is sufficiently small (in particular if $h^2\|U_h\|_\infty^8$ is small), then

$$\frac{\big|\|u\|_\infty - \|U_h\|_\infty\big|}{\|U_h\|_\infty} \approx \frac{Ch^2\|U_h\|_\infty^8}{2\lambda}. \tag{1.5}$$

Observe the rapid growth in this estimate as $\|U_h\|_\infty$ increases. If h satisfies the less restrictive requirement that $h^2\|U_h\|_\infty^4$ is small, then

$$\|u\|_\infty \approx \frac{\|U_h\|_\infty}{\sqrt{1 - Ch^2\|U_h\|^8/\lambda}}, \tag{1.6}$$

which reduces to (1.5) in the limit of small h. In contrast, if $\lambda = \lambda_0$ so that the numerical solution is spurious we have that

$$\|U_h\|_\infty \approx \left(\frac{\lambda_0}{C}\right)^{1/8} h^{-1/4} \tag{1.7}$$

so that $\|U_h\|_\infty$ grows slowly as h decreases. The value of C depends upon the elements used but not upon the domain and can be calculated a priori. Consequently, these results have immediate extensions to problems with more complex geometries.

Although the restriction that $h^2\|U_h\|_\infty^4$ be small means that we must use a moderately fine mesh for these results to be sharp when $\|U_h\|_\infty$ is large, the restriction is not too severe and we are able to perform computations with such meshes for which (1.6) is sharp. Using this formula we derive in section 7 a procedure for post-processing the results to obtain a more accurate value for $\|u\|_\infty$ and hence to estimate λ_0. This post-processing can be applied to results for more complex domains and for more general nonlinearities which grow at the critical rate. The post-processing procedure is much easier to apply and more effective than the use of adaptive methods, giving accurate numerical approximations and rejecting spurious solutions while using meshes for which computations are feasible.

As an application of these methods we give computational evidence to support a conjecture made by McLeod [13] that λ_0 is equal to a value λ_{**} obtained by solving a related linear problem. (This is the value of λ indicated in Figure 1.1.) We also give strong evidence to show that the solutions in the cube are unique and have a high degree of radial symmetry away from the boundary.

The layout of the remainder of this paper is as follows. In section 2 we give a brief summary of the significant analytic results and conjectures concerning (1.1) and in particular describe the form of the developing singularity. In section 3 we derive the finite element method and state some known results on its convergence. In section 4 we apply this method to solve a linear problem which approximates (1.1) when u is large. This gives both an upper bound and an estimate λ_{**} for λ_0. In section 5 we compute solutions for the full problem (1.1) and present the results, indicating that for sufficiently fine meshes the solutions obey a scaling law. In section 6 we apply formal asymptotic techniques to derive an improved description of both u and U_h. Finally, in section 7, we use the asymptotic formula to derive the estimates (1.5), (1.6), (1.7) and then apply (1.6) to post-process the numerical results to obtain a more accurate description of the solution.

2. The qualitative form of the analytic solution branch.

2.1. Existence. We define bilinear operators $a(u,v)$ and $\langle u,v\rangle$ by

$$a(u,v)=\int_\Omega \nabla u.\nabla v\,d\Omega \qquad \text{and} \qquad \langle u,v\rangle=\int_\Omega uv\,d\Omega$$

and denote by $H_0^1(\Omega)$ the usual Sobolev space of functions vanishing on the boundary of Ω with norm defined by $\|u\|_{H_0^1}^2=a(u,u)$. Furthermore, let $\lambda_1(\Omega)$ be the smallest eigenvalue, with positive eigenfunction vanishing on the boundary of Ω, of the differential operator $-\Delta$. A weak solution $u\in H_0^1(\Omega)$ of the general problem

$$\left.\begin{array}{ll}\Delta u+\lambda u+u^p=0 & \text{on } \Omega\subset\mathbb{R}^3,\\ u>0 & \text{in } \Omega,\\ u=0 & \text{on } \partial\Omega\end{array}\right\} \tag{2.1}$$

is a zero of the function $\Psi: H_0^1(\Omega)\to H^{-1}(\Omega)$ defined by

$$\Psi(u)\varphi=-a(u,\varphi)+\langle \lambda u+u^p,\varphi\rangle. \tag{2.2}$$

If $\lambda<\lambda_1$, then a sufficient condition (see, for example, [7]) for the existence of such a (nontrivial) weak solution is that $H_0^1(\Omega)$ is compactly embedded in $L^{p+1}(\Omega)$. For the *subcritical* case $p<5$, this condition holds and the variational approach predicts that solutions of (1.1) exist for all $\lambda<\lambda_1$. The theory for this case is reviewed in Lions [11].

For the *critical* case $p = 5$, $H_0^1(\Omega)$ is embedded in $L^{p+1}(\Omega)$ but this embedding is not compact and the existence of solutions cannot be guaranteed. Some extensions to the existence theory in this case are given by [2] and [14].

2.2. The solution branch. It is a straightforward application of bifurcation theory to show that if $p > 1$ a solution branch (λ, u) of (2.1) bifurcates from the trivial solution $u = 0$ at $\lambda = \lambda_1(\Omega)$. This branch is unbounded in the joint norm of $|\lambda| + \|u\|_\infty$, exists in a left neighborhood of λ_1, and is restricted to lie in the region $\lambda < \lambda_1$. Following the important result in [10] we may also deduce that the function u inherits the symmetries of Ω. Brezis and Nirenberg [2] showed that when $p = 5$, for any star-shaped domain there exists a critical value $\lambda_0 = \lambda_0(\Omega) > 0$ such that λ_0 is the infimum of the set of values of λ for which (1.1) has a solution. In [2] various upper bounds for λ_0 are given; in particular it is shown that a solution exists if

$$\lambda \geqslant \lambda_* \equiv \frac{\pi^2}{4R^2}, \tag{2.3}$$

where R is the radius of the largest ball that can be placed inside Ω.

2.3. The nature of the singularity. For the sphere it is known that $\|u\|_\infty \to \infty$ as $\lambda \to \lambda_0$ [2] and it is conjectured that if Ω is a star-shaped domain, then $u(\mathbf{x})$ is a unique function of λ for $\lambda \in (\lambda_0, \lambda_1)$, which becomes infinite at a single point $\mathbf{x_0}$ as λ tends to λ_0 and which tends to zero at all other points. It is not known if this conjecture is true even for simple domains such as the cube or cuboid. The solution profiles presented in Figure 1.2 lend some support to this conjecture as they show a narrowing peak developing at the center of the cube as λ is reduced, although (due to the errors in the numerical computation) there is no point λ_0 at which the illustrated solution becomes unbounded. As u is large at $\mathbf{x}_0$ the u^5 term in (1.1) dominates λu at this point. Elsewhere, where u is small, λu dominates u^5. Using this result we can crudely approximate the function u^5 in (1.1) by a scalar multiple $A\delta(\mathbf{x} - \mathbf{x_0})$ of the delta function leading to the approximation

$$\Delta u + \lambda u = -A\delta(\mathbf{x} - \mathbf{x}_0). \tag{2.4}$$

This equation has the solution

$$u(\mathbf{x}) \approx AG_\lambda(\mathbf{x}, \mathbf{x_0}), \tag{2.5}$$

where G_λ is the Green's function for the Helmholtz operator $-\Delta u - \lambda u$. In section 5 we derive an approximate value for A and compare (2.5) with the calculated solution. By studying this equation, McLeod [13] (see also [16], [1]) proved an upper estimate λ_{**} for λ_0. For the sphere it is known that $\lambda_{**} = \lambda_0$, and McLeod conjectured that this result will also hold for more general domains. For the cube, the value of λ_{**} can be computed accurately fairly easily, and we detail this calculation and give a precise definition for λ_{**} in section 4. We then show that, up to the accuracy that we can compute λ_0 for the cube, the values of λ_0 and λ_{**} are equal.

The approximation (2.4) is crude and the description of the solution can be improved by using some scaling arguments. To do this we presume (without loss of generality) that the maximum value of $u(\mathbf{x})$ occurs at the origin and define

$$\gamma = \|u\|_\infty = u(\mathbf{0}).$$

Now introduce the scaled function $v(\mathbf{y})$ and scaled coordinate $\mathbf{y}$ defined by

$$u(\mathbf{x}) = \gamma v(\gamma^2 \mathbf{x}) \quad \text{and} \quad \mathbf{y} = \gamma^2 \mathbf{x}. \tag{2.6}$$

Rescaling (1.1) and expressing all derivatives in terms of $\mathbf{y}$ we have

$$\Delta v + v^5 + \lambda\gamma^{-4} v = 0, \quad \|v\|_\infty = 1, \tag{2.7}$$

where $v = 0$ on $\partial\Omega_\gamma$ with Ω_γ a rescaling of Ω. For large γ, v approximately satisfies the simpler equation $\Delta v + v^5 = 0$ which, in the absence of boundary conditions, has the radially symmetric solution

$$w(\mathbf{y}) = \left(1 + \frac{|\mathbf{y}|^2}{3}\right)^{-1/2}. \tag{2.8}$$

If γ is large, then the boundary of Ω_γ is distant from the origin and can be expected to have only a small effect on the solution of (2.7). We make the reasonable conjecture that close to the origin v is also close to being radially symmetric and hence that $v(\mathbf{y}) \approx w(\mathbf{y})$. Rescaling this gives

$$u(\mathbf{x}) \approx w_\gamma(\mathbf{x}) \equiv \frac{\gamma}{(1 + \frac{1}{3}\gamma^4|\mathbf{x}|^2)^{1/2}}. \tag{2.9}$$

The expression (2.9) gives a leading order approximation to $u(\mathbf{x})$ close to the singularity which becomes progressively less accurate as $\mathbf{x}$ approaches the boundary of Ω; however, the computations presented in section 5 demonstrate that (2.9) is very descriptive for even quite large values of $|\mathbf{x}|$.

3. Qualitative properties of the discrete equations. We now describe the basic finite element method used to calculate a discrete solution branch (λ, U_h) approximating the true solution branch (λ, u) of (1.1). We then make some preliminary observations about the underlying behavior of the discrete solution and the problems encountered as the true solution becomes more singular.

3.1. Formulation of the finite element equations. The finite element method seeks a zero of the functional Ψ defined in (2.2) but now considered as a map from a *finite-dimensional* subspace $S_h(\Omega)$ of $H_0^1(\Omega)$ to its dual space $S_h^{-1}(\Omega)$. This is equivalent to finding a function $U_h \in S_h$ such that

$$-a(U_h, \varphi) + \langle \lambda U_h + U_h^5, \varphi\rangle = 0 \quad \forall \varphi \in S_h. \tag{3.1}$$

In contrast to the situation for (2.2), the space S_h is finite dimensional, and so the embedding of S_h into L^{p+1} is compact for all values of $p \geqslant 1$. As a consequence we can deduce the following result.

THEOREM 3.1. *A positive solution branch* $(\lambda, U_h) \in \mathbb{R} \times S_h$ *of* (3.1) *exists* $\forall p \geqslant 1$ *and* $\forall \lambda < \lambda_1$.

Proof. The proof follows immediately from the mountain pass lemma (see [7]). More details are given in [5]. □

If $\lambda > \lambda_0$, then such solutions should converge to the true solution of the underlying problem as the computational mesh is refined. However, if $\lambda < \lambda_0$, then they cannot converge, as no true solution exists, and thus are spurious. Now take Ω to be a cube centered on the origin with $-1/2 \leqslant x, y, z \leqslant 1/2$. We divide Ω into a regular lattice of cubic elements of side h with $S_h \subset H_0^1(\Omega)$ the space spanned by the basis functions $\varphi_i(\mathbf{x})$ which have as support the eight elements centered on the ith node, are trilinear on these elements (i.e., linear in each coordinate direction), are continuous

across the element boundaries, take the value 1 at the ith node, and are zero at all other nodes. Thus we may represent $U_h(\mathbf{x})$ as

$$U_h(\mathbf{x}) = \sum_{i=1}^{N} U_i \varphi_i(\mathbf{x})$$

and rewrite (3.1) as

$$-\sum_{i=1}^{N} U_i a(\varphi_i, \varphi_j) + \langle \lambda U_h + U_h^5, \varphi_j \rangle = 0 \quad \forall j = 1, \ldots, N. \tag{3.2}$$

For this calculation, the simple polynomial nature of the nonlinearity means that all integrals can be evaluated exactly by using Gaussian quadrature on each element with four integration points in each coordinate direction. The finite element method thus reduces the problem (3.1) to solving N coupled (nonlinear) equations for the unknowns $\boldsymbol{U} = [U_1, \ldots, U_n]^T \in \mathbb{R}^n$ and we rewrite (3.2) as

$$K\mathbf{U} = \lambda A\mathbf{U} + \mathbf{G}(\mathbf{U}), \tag{3.3}$$

where $K_{ij} = a(\varphi_i, \varphi_j)$, $A_{ij} = \langle \varphi_i, \varphi_j \rangle$, and $[\mathbf{G}(\mathbf{U})]_i = \langle U_h^5, \varphi_i \rangle$. By solving (3.3) we can thus find a *branch* (λ, U_h) of solutions of the discrete weak equation (3.1). The arguments presented in [15] show that the branch so computed satisfies

$$\|U_h\|_\infty < Ch^{-1/2},$$

where C depends upon the domain, but not on λ, h, or U_h.

As will be clear in section 5, it is necessary to take $N \approx 10^6$ nodes, which leads to severe computational difficulties in solving the algebraic systems. Our technique for finding the solution is to exploit the natural homotopy parameter λ and solve (3.3) by numerical continuation in this parameter given a suitable starting point, and making small reductions in λ at each step. For each such step we solve (3.3) by using a pseudo-Newton method for which the Jacobian of the problem is approximated by a related matrix with reduced memory allocation. These pseudo-Jacobian matrices are symmetric but not positive definite. The resulting linear systems are then solved by using the conjugate gradient method *without* preconditioning. There are two reasons why preconditioning is not used. First, standard preconditioners are ineffective because the pseudo-Jacobian matrices are not positive definite, and second, the unconditioned method converges relatively quickly. For an unpreconditioned system if the indefiniteness causes difficulties with the convergence of the conjugate gradient (CG) method, then this is readily seen. Although CG is robust only for positive definite systems, we found no convergence difficulties for our (mildly) indefinite problems. For example, on a mesh of $100^3 = 10^6$ elements making a step of $\Delta\lambda = 0.5$ between successive values of λ, on average only 1.32 iterations of the Newton method and 210 inner iterations of the CG method are needed to obtain a convergent solution at each step.

3.2. Starting the branch. An application of standard bifurcation theory to the discrete problem (3.3) implies that there is a bifurcation of a nontrivial solution branch from the zero solution at the value $\lambda = \lambda_{1,h}$, where $\lambda_{1,h}$ is the smallest generalized eigenvalue of the system linearized about $\mathbf{U} = \mathbf{0}$ satisfying

$$K\psi_{1,h} = \lambda A\psi_{1,h}$$

with a nonzero vector $\psi_{1,h}$. This equation is a discretization of the Helmholtz equation $-\Delta\psi_1 = \lambda\psi_1$, $\psi = 0$ if $\mathbf{x} \in \partial\Omega$ satisfied (for nonzero ψ) when $\lambda = \lambda_1(\Omega)$ and from standard results in approximation theory we have that $\lambda_1 < \lambda_{1,h} = \lambda_1 + \mathcal{O}(h^2)$. For the unit cube $\lambda_1 = 3\pi^2$ and

$$\psi_1(\mathbf{x}) = \psi_1(x, y, z) = \cos(\pi x)\cos(\pi y)\cos(\pi z).$$

Taking $\lambda = \lambda_1$ initially and setting $U_h = \hat{\psi}_1$ with $\hat{\psi}_1$ the interpolant of ψ_1 in S_h proved a sufficiently accurate initial guess to allow rapid convergence onto the solution branch.

3.3. Convergence of the numerical method. The study of the convergence of the discretizations of general semilinear equations is not new. An overall theory (based upon the implicit function theorem or on concepts of nonlinear stability) has been developed for the numerical approximation of isolated solutions of problems of the form (1.1) for fairly general functions $f(u;\lambda)$. Good references to this work are given in the monograph by Crouzeix and Rappaz [8] and also in the papers by Lopez-Marcos and Sanz-Serna [12] and Dobrowolski and Rannacher [9]. Such results typically assume that a solution U_h has been constructed in a neighborhood of the true solution u and look at the convergence of U_h to u as the mesh is refined. For piecewise linear finite elements, we have [9]

$$\|U_h - u\|_\infty < B_\infty(u)h^2\log(1/h), \quad \|U_h - u\|_{H_0^1} < B_H(u)h \quad \text{as} \quad h \to 0. \tag{3.4}$$

In Lopez-Marcos and Sanz-Serna [12] it is also shown that there exist neighborhoods of u (called *stability balls*) in which U_h both exists and is unique. In Murdoch and Budd [15] these results were applied directly to problems of the form (1.1) and it was shown that the radii of the stability balls were mesh dependent and that spurious solutions could exist outside them. For the estimates of $\|U_h - u\|_\infty$ the constant $B_\infty(u)$ is proportional both to $\|\Delta u\|_\infty = \|\lambda u + u^5\|_\infty$ and to the infinity norm of the operator L_λ^{-1} defined in (1.4). Because both are unbounded as $\lambda \to \lambda_0$ the above estimate is hard to apply, and descriptive only when h is very small. Consequently, the result (3.4) does not give a completely satisfactory account of the convergence of a numerical method for (1.1).

3.4. Spurious solutions of the numerical method. A secondary difficulty arises with spurious solutions when $\lambda < \lambda_0$. Obviously, it is important to distinguish such solutions from convergent approximations to solutions of (1.1). In particular, they diverge to infinity in $L^\infty(\Omega)$ as the mesh is refined but remain bounded in other norms. Indeed, we observe spurious solutions of (1.1) which remain bounded in $H_0^1(\Omega)$ under mesh refinement and tend to zero in $L^2(\Omega)$. As mentioned in the introduction, the divergence in L_∞ as the mesh is refined can be very slow; typically for spurious solutions of (1.1) we will see that $\|U_h\|_\infty \sim h^{-1/4} \sim N^{1/12}$ where N is the number of computational nodes. With such a slow rate of divergence it is not computationally feasible to use fine enough meshes to clearly distinguish between a slowly growing spurious solution and a convergent solution. This motivates the calculations in section 6 where asymptotic methods are used to distinguish between the two types of solution.

3.5. Resolution of the singularity. The main difficulty posed to the numerical method is an adequate resolution of the singularity as $\lambda \to \lambda_0$. A preliminary error analysis can be made by considering the rescaling (2.6) which can also be applied to the finite element discretization. In particular, suppose that

$$\gamma = \|U_h\|_\infty, \quad \mathbf{y} = \gamma^2\mathbf{x} \text{ and } U_h(\mathbf{x}) = \gamma V_H(\gamma^2\mathbf{x}), \tag{3.5}$$

where

$$H = \gamma^2 h. \tag{3.6}$$

Under this rescaling $V_H(\mathbf{y})$ belongs to the space of functions spanned by piecewise trilinear basis functions defined on cubes of side H. In the rescaled variables, we have conjectured that close to its peak the rescaled function $v(\mathbf{y})$ has the approximate form

$$v(\mathbf{y}) \approx 1/(1 + |\mathbf{y}|^2/3)^{1/2}.$$

For V_H to approximate this function it is clearly necessary that $H \ll 1$. Standard error estimates then imply that we can approximate $v(\mathbf{y})$ to an accuracy of $\mathcal{O}(H^2)$ by using piecewise linear elements and hence, on the original mesh, we can approximate the rescaled function $w_\gamma(\mathbf{x})$ to an accuracy of $\mathcal{O}(h^2\gamma^5)$. Thus, a necessary condition for an accurate numerical solution of (1.1) is that H is small. Now observe that whereas h is known, the value of H can only be determined subsequent to the computation. Moreover, the condition of H being small is not sufficient since we have no a priori guarantee that the value of γ itself is correct. Thus, although the numerical method may be able to resolve the profile of the singularity, it may get its maximum value wrong. This turns out to be a second principal source of error, and we return to this in sections 5 and 6.

4. Critical values of λ derived from the linear Green's function.

4.1. McLeod's conjecture. For our first investigations of the solutions of the nonlinear partial differential equation problem (1.1) we study the solutions of the related *linear* problem (2.4) approximating (1.1) when u is large. A numerical study of this problem is rather simpler than that for (1.1) and yet gives insight into the behavior of the large solutions and affords the possibility of determining the range of existence of the solutions of (1.1) without solving the fully nonlinear problem.

For general $\mathbf{x}$, $\mathbf{y}$ the Green's function for the Helmholtz operator satisfies the equation

$$\left.\begin{aligned} \Delta G_\lambda(\mathbf{x},\mathbf{y}) + \lambda G_\lambda(\mathbf{x},\mathbf{y}) &= -\delta(\mathbf{x}-\mathbf{y}), \qquad \mathbf{x} \in \Omega, \\ G_\lambda(\mathbf{x},\mathbf{y}) &= 0, \qquad \mathbf{x} \in \partial\Omega \end{aligned}\right\} \tag{4.1}$$

(where all spatial derivatives are expressed in terms of $\mathbf{x}$). Since

$$\Delta\left(\frac{1}{4\pi|\mathbf{x}-\mathbf{y}|}\right) = -\delta(\mathbf{x}-\mathbf{y}) \tag{4.2}$$

we may write

$$G_\lambda(\mathbf{x},\mathbf{y}) = \frac{1}{4\pi|\mathbf{x}-\mathbf{y}|} + g_\lambda(\mathbf{x},\mathbf{y}), \tag{4.3}$$

where the continuous but nonsmooth function $g_\lambda(\mathbf{x},\mathbf{y})$ is called the *regular part* of the Green's function. It follows from (4.1) and (4.3) that

$$\left.\begin{aligned} \Delta g_\lambda(\mathbf{x},\mathbf{y}) + \lambda g_\lambda(\mathbf{x},\mathbf{y}) &= -\frac{\lambda}{4\pi|\mathbf{x}-\mathbf{y}|}, \qquad \mathbf{x} \in \Omega, \\ g_\lambda(\mathbf{x},\mathbf{y}) &= -\frac{1}{4\pi|\mathbf{x}-\mathbf{y}|}, \qquad \mathbf{x} \in \partial\Omega. \end{aligned}\right\} \tag{4.4}$$

Following Brezis [1] we define the function $\varphi_\lambda(\mathbf{x}) \equiv g_\lambda(\mathbf{x},\mathbf{x})$. McLeod [13] and Schoen [16] showed independently that if $\varphi_\lambda(\mathbf{x}) > 0$ for some point $\mathbf{x}$ in Ω, then (1.1) has a solution. In [1] it is shown that $\varphi_\lambda(\mathbf{x})$ increases with λ and hence there is a unique $\lambda = \lambda_{**}$ and an $\mathbf{x_0} \in \Omega$, such that

$$\max(\varphi_\lambda(\mathbf{x}) : \mathbf{x} \in \Omega) = \varphi_\lambda(\mathbf{x}_0) = 0 \quad \text{if} \quad \lambda = \lambda_{**}.$$

Hence we have the following result.

LEMMA 4.1. *The problem* (1.1) *has a solution if* $\lambda > \lambda_{**}$.

McLeod conjectured that $\lambda_{**} = \lambda_0$. Strong numerical evidence supporting this conjecture is presented in the rest of this paper.

It is clear from the discussion above that a numerical computation of the function $g_\lambda(\mathbf{x},\mathbf{y})$ and hence of $\varphi_\lambda(\mathbf{x})$ has the potential of giving much insight into the solutions of (1.1). This computation requires the solution of a linear problem, which can be determined with great accuracy at relatively little cost. In cuboid domains centered on the origin, symmetry arguments imply that $\mathbf{x_0} = \mathbf{0}$ and hence we need only compute $\varphi_\lambda(\mathbf{0})$.

Equation (4.4) has a singularity as $|\mathbf{x}-\mathbf{y}| \to \mathbf{0}$ making computation difficult. Consequently, we solve a related problem which removes this singularity. In contrast to (4.3) we write

$$G_\lambda(\mathbf{x},\mathbf{y}) = \theta_\lambda(\mathbf{x},\mathbf{y}) + h_\lambda(\mathbf{x},\mathbf{y}), \quad \text{where} \quad \theta_\lambda(\mathbf{x},\mathbf{y}) = \frac{\cos(\lambda^{1/2}|\mathbf{x}-\mathbf{y}|)}{4\pi|\mathbf{x}-\mathbf{y}|}. \tag{4.5}$$

A simple calculation shows that

$$\Delta\theta_\lambda(\mathbf{x},\mathbf{y}) + \lambda\theta_\lambda(\mathbf{x},\mathbf{y}) = -\delta(\mathbf{x}-\mathbf{y}), \tag{4.6}$$

and substituting (4.5) into (4.1) and using (4.6) we obtain

$$\left.\begin{array}{ll} \Delta h_\lambda(\mathbf{x},\mathbf{y}) + \lambda h_\lambda(\mathbf{x},\mathbf{y}) = 0, & \mathbf{x} \in \Omega, \\ h_\lambda(\mathbf{x},\mathbf{y}) = -\theta_\lambda(\mathbf{x},\mathbf{y}), & \mathbf{x} \in \partial\Omega. \end{array}\right\} \tag{4.7}$$

If $\mathbf{y} \notin \partial\Omega$, then the function θ_λ is smooth on the boundary of $\partial\Omega$. Thus, if $\lambda < \lambda_1$, standard results from the theory of elliptic partial differential equations predict that the function h_λ exists and is smooth in the interior of Ω. Finally, using (4.3) and (4.5) it follows that

$$g_\lambda(\mathbf{x},\mathbf{y}) = \frac{1}{4\pi|\mathbf{x}-\mathbf{y}|}\Big(\cos(\lambda^{1/2}|\mathbf{x}-\mathbf{y}|) - 1\Big) + h_\lambda(\mathbf{x},\mathbf{y}). \tag{4.8}$$

To compute λ_{**} for cuboid domains with $\mathbf{x_0} = \mathbf{0}$ we solve (4.7) for $h_\lambda(\mathbf{x},0)$ using the finite element method with the same mesh and basis functions as in section 3. Letting $\mathbf{x} \to \mathbf{0}$ in (4.8) then gives

$$\varphi_\lambda(\mathbf{0}) = g_\lambda(\mathbf{0},\mathbf{0}) = h_\lambda(\mathbf{0},\mathbf{0}). \tag{4.9}$$

The value of λ_{**} is determined by using path following in λ and interval bisection to find the unique value for which $\varphi_{\lambda_{**}}(\mathbf{0}) = 0$. We note that as the function h_λ is smooth, then standard error estimates of the form (3.4) from the theory of the finite element method may be applied to estimate the accuracy of the above computation. As the value of θ_λ on $\partial\Omega$ depends smoothly upon λ, as does the inverse of the linear operator in (4.8), the constants implied in these calculations (unlike those in the calculation of the nonlinear equation) are largely independent of λ, and consequently we predict a consistently accurate solution.

TABLE 4.1
Computed values $\lambda_{**}(h)$, where Ω is a cube of side 1 using the finite element method with mesh size h.

h	$\lambda_{**}(h)$	C	λ_{**}
1/10	7.421711		
1/20	7.483804	8.279	7.504502
1/30	7.495309	8.283	7.504513
1/40	7.499337	8.287	7.504516
1/50	7.501201	8.284	7.504515
1/60	7.502212	8.271	7.504510
1/70	7.502823	8.289	7.504514
1/80	7.503220	8.304	7.504518
1/90	7.503491	8.259	7.504511
1/100	7.503685	8.274	7.504512
1/110	7.503829	8.297	7.504515

4.2. Results. Table 4.1 presents calculated values of λ_{**} for Ω is a cube of side 1, using the finite element method described in section 3. Here, $\lambda_{**}(h)$ is the numerical approximation to λ_{**} obtained by using mesh of side h.

Studying Table 4.1, we have strong evidence that asymptotically

$$\lambda_{**} = \lambda_{**}(h) + Ch^2 + \mathcal{O}(h^3), \tag{4.10}$$

consistent with the second order convergence of the finite element method when using trilinear basis functions. Using two successively finer meshes we estimate C and λ_{**} to give the numbers in the third and fourth columns of the table. These strongly imply that for a cube of side 1

$$\lambda_{**} \approx 7.5045. \tag{4.11}$$

5. Finite element solutions of the full nonlinear problem. We now return to the nonlinear problem (1.1) and present the results of some computations. An asymptotic analysis of these computations is given in section 6. By computing the bifurcation diagram for $(\lambda, \|U_h\|)$ in various norms we can investigate the solution (and in particular the formation of the singularity) for a range of values of λ. A preliminary guide to the accuracy of this calculation is given by the local analysis of section 3 which showed that the developing peak can be realistically resolved only if H as defined in (3.5) is small. Consequently, we label the corresponding meshes as *coarse* and *fine* depending upon the resulting value of H. An immediate difficulty with this computation is that whereas the value of h is known a priori, the value of γ (which is a strongly nonlinear function of h) and a mesh can be classified only as coarse or fine subsequent to a numerical calculation. As discussed in section 3, having a fine mesh does not guarantee the accuracy of the calculation. However, we show that the solutions on the fine meshes obey scaling laws making them amenable to asymptotic analysis.

5.1. Coarse mesh solutions. Our initial calculations for (1.1) were made with a mesh varying from $h = 1/10$ to $h = 1/50$. While the case of $h = 1/10$ corresponds to 10^3 elements and can certainly be regarded as coarse, a mesh with $h = 1/50$ has 1.25×10^5 elements and may intuitively be regarded as fine. However, results on this mesh, although looking reasonable, are misleading as H is large. We present these results here to give some insight into the nature of truly spurious solutions which do not in any way resolve the singularity in u and from which little useful information can be extracted, leaving calculations on finer meshes to the next subsection.

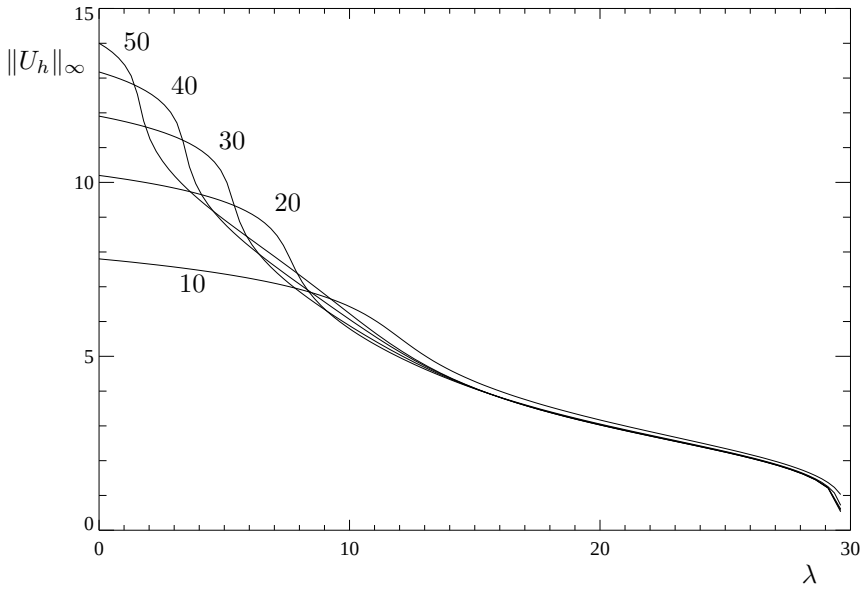

FIG. 5.1. *Bifurcation diagram of* $\|U_h\|_\infty$ *against* λ *for coarse grids varying between* $h = 1/10$ *and* $h = 1/50$.

From Figure 5.1 it is evident that a solution branch of the numerical discretization exists for all $\lambda < \lambda_1$. A steep gradient forms in each figure and the value of λ at which this occurs decreases as the mesh is refined. This gives the misleading picture that λ_0 is close to zero. However, we observe that as the mesh is refined, there is little agreement among any of the curves when $\lambda \leqslant 13$ and the structures observed for this range of λ should be viewed with suspicion. A qualitative indication of this is the nonmonotonicity of the graph of $\|U_h\|_\infty$ under mesh refinement, leading to a braiding structure in the bifurcation diagram.

A useful measure of the error of the solution is given by the value of H when $\lambda = \lambda_{**}$. In particular we have $H = 4.914$ if $h = 1/10$ and $H = 1.157$ if $h = 1/50$.

5.2. Bifurcation diagrams for the fine mesh solutions in various norms. We now look at computations on finer meshes for which H takes smaller values than previously and for which the results obey a detectable asymptotic scaling law as $h \to 0$.

5.2.1. The maximum norm. A plot of $\|U_h\|_\infty$ against λ for values of the mesh size from $h = /60$ to $h = 1/100$ (10^6 elements) was presented in Figure 1.1. The solution branches for all these meshes agree for $\lambda \gtrapprox 12$, and for smaller values of λ this figure is strikingly different from Figure 5.1. Excepting the case of the $h = 1/60$ branch near $\lambda = 0$, we see that the value of $\|U_h\|_\infty$ is monotonically increasing as the mesh is refined, avoiding the braiding seen earlier. In this case the value of H when $\lambda = \lambda_{**}$ decreases from $H = 1.032$ when $h = 1/60$ to $H = 0.774$ when $h = 1/100$. Although this value is still not very small, it appears to be small enough for the asymptotic theory we will develop to be descriptive. It is revealing to also plot $1/\|U_h\|_\infty^2$. This is given in Figure 5.2.

For the sphere it is shown in [4], [3] that $1/\|u\|_\infty^2$ is proportional to $\lambda - \lambda_0$ if λ is close to λ_0. In Figure 5.2 we see that the corresponding curve for $1/\|U_h\|_\infty^2$ in

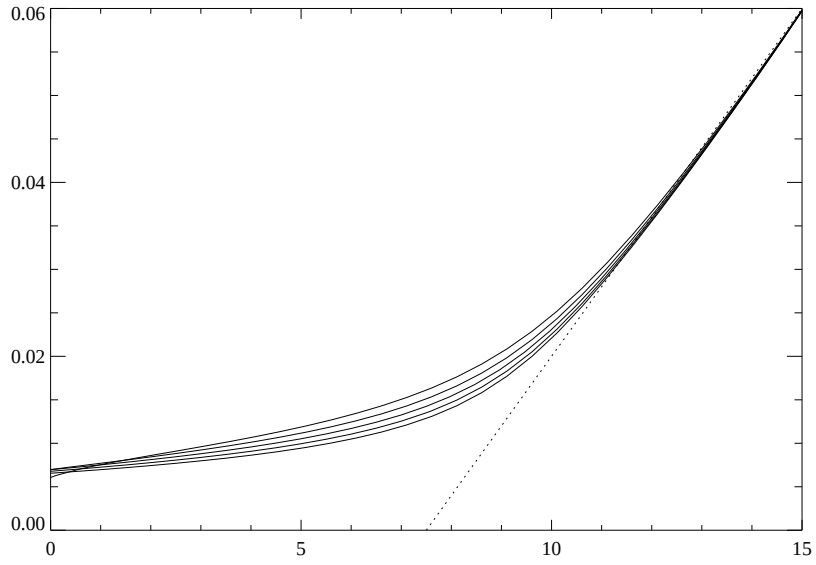

FIG. 5.2. *Bifurcation diagram of* $1/\|U_h\|_\infty^2$ *against* λ *for grids varying between* $h = 1/60$ *and* $h = 1/100$. *For moderate values of* λ ($\lambda \in [5, 10]$) *the value of* $1/\|U_h\|_\infty^2$ *decreases monotonically as the mesh is refined.*

TABLE 5.1
Computed values of $\|U_h\|_\infty$ *for various values of* λ *and various mesh sizes.*

Mesh	λ										
size	0	1	2	3	4	5	6	7	8	9	10
1/10	*7.80*	*7.73*	*7.65*	*7.57*	*7.47*	*7.37*	*7.24*	*7.10*	*6.92*	*6.71*	*6.43*
1/20	*10.20*	*10.10*	*9.98*	*9.84*	*9.67*	*9.44*	*9.13*	*8.56*	*7.27*	*6.36*	5.79
1/30	*11.91*	*11.75*	*11.57*	*11.32*	*10.95*	*10.17*	*8.32*	7.47	6.86	6.35	5.88
1/40	*13.18*	*12.93*	*12.57*	*11.86*	*9.76*	8.82	8.16	7.60	7.08	6.57	6.06
1/50	*14.00*	*13.40*	*11.30*	10.20	9.50	8.92	8.39	7.87	7.34	6.79	6.23
1/60	*12.84*	*11.51*	10.79	10.21	9.68	9.18	8.68	8.15	7.59	6.99	6.37
1/70	11.97	11.39	10.89	10.41	9.94	9.47	8.97	8.43	7.83	7.18	6.48
1/80	11.98	11.53	11.10	10.66	10.22	9.75	9.24	8.69	8.05	7.34	6.58
1/90	12.14	11.74	11.34	10.92	10.49	10.03	9.51	8.93	8.25	7.48	6.66
1/100	12.35	11.98	11.60	11.19	10.76	10.29	9.77	9.16	8.44	7.61	6.73

the cube is approximately linear for $12 < \lambda < 15$ but departs from linearity as λ is reduced. Extrapolating the linear section gives an intercept (indicated) at a value of λ close to λ_{**}. In section 7 we will demonstrate much stronger reasons for believing that $\lambda_0 = \lambda_{**}$. In Table 5.1 we present a table of $\|U_h\|_\infty$ for various values of λ between 0 and 10, with mesh sizes between $h = 1/10$ and $h = 1/100$. For any fixed value of λ in the table the value of $\|U_h\|_\infty$ is ultimately monotonically increasing as the mesh is refined; however, the smaller the value of λ, the finer the mesh must be taken before this monotonicity is observed and any scaling law becomes apparent.

Table 5.1 clearly indicates the difficulties in determining the difference between a convergent and a spurious solution. For $\lambda > \lambda_{**} = 7.5045$, Lemma 4.1 gives the existence of a solution of (1.1) and consequently U_h will converge toward this solution as $h \to 0$. However, it is almost impossible from an a priori inspection to differentiate

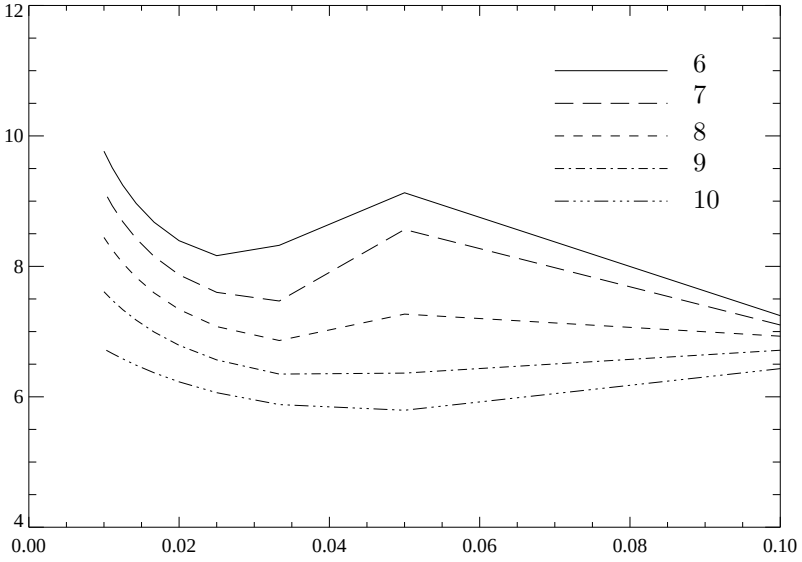

FIG. 5.3. *The value of* $\|U_h\|_\infty$ *as a function of* h *in the cases of* $\lambda = 6, 7, 8, 9, 10$.

TABLE 5.2
$\|U_h\|_\infty$ *and* $h^{1/4}\|U_h\|_\infty$ *on various meshes.*

h	$\|U_h\|_\infty$	$h^{1/4}\|U_h\|_\infty$	p	K
1/10	7.018735	3.947		
1/20	7.992000	3.779	−0.1873	4.559
1/30	7.146795	3.054	0.2757	18.252
1/40	7.334479	2.916	−0.0901	5.260
1/50	7.604458	2.860	−0.1620	4.035
1/60	7.875852	2.830	−0.1923	3.583
1/70	8.133509	2.812	−0.2088	3.349
1/80	8.374874	2.8 00	−0.2190	3.208
1/90	8.600438	2.792	−0.2256	3.116
1/100	8.811953	2.787	−0.2306	3.047

between a convergent solution at $\lambda = 8$ and a potentially spurious solution at $\lambda = 7$. To demonstrate this we plot in Figure 5.3 the value of $\|U_h\|_\infty$ for $\lambda = 6, 7, 8, 9, 10$ as h is refined, noting that the latter three graphs all correspond to convergent solutions. For sufficiently small h each of these graphs takes on a regular appearance which appears to indicate a regular and slow growth in $\|U_h\|_\infty$ as h is reduced, although we note that this is not inconsistent with convergence, only that h is not sufficiently small for convergence to be apparent for the meshes used.

Now taking $\lambda = \lambda_{**}$ we study this asymptotic growth in more detail. In Table 5.2 we present $\|U_h\|_\infty$ and $h^{1/4}\|U_h\|_\infty$ for varying h and also estimates of K and p obtained by applying the formula $\gamma = Kh^p$ to successive entries in the table through $p = (\log(\|U_{h_1}\|_\infty) - \log(\|U_{h_2}\|_\infty))/(\log h_1 - \log h_2)$ and $K = (\|U_{h_2}\|_\infty)(h_2^p)$. These results imply strongly that p is close to $-1/4$ and are fully consistent with the predictions of the formal asymptotic formula (1.7).

More generally the results in section 7 imply that if λ is close to but larger than λ_0, then for h lying in the range $\|u\|_\infty^{-4} \ll h \ll \|u\|_\infty^{-2}$ the value of $\|U_h\|_\infty$ grows as $h^{-1/4}$ before converging to $\|u\|_\infty$ for smaller values of h.

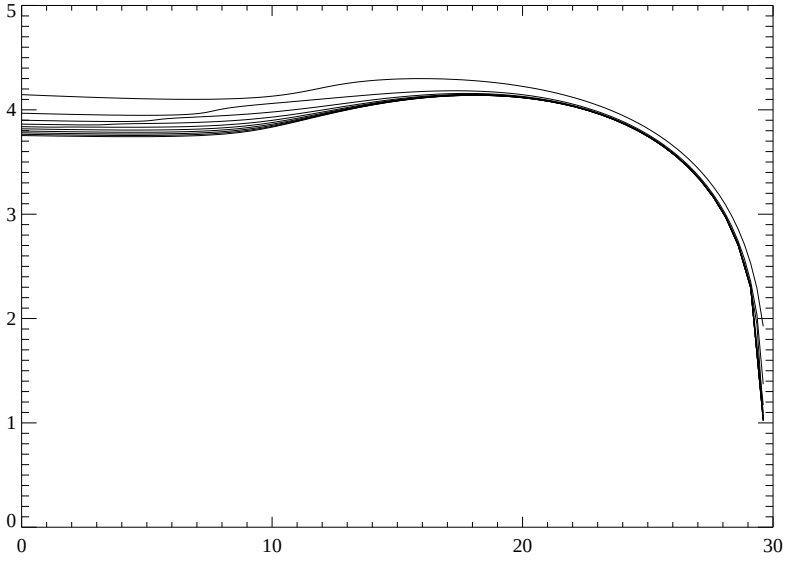

FIG. 5.4. *Bifurcation diagram of* $\|U_h\|_{H_0^1}$ *against* λ, *for grids varying between* $h = 1/10$ *and* $h = 1/100$. *The value of* $\|U_h\|_{H_0^1}$ *is monotonically decreasing as the mesh is refined.*

5.2.2. The Sobolev norm. In Figure 5.4 we display the solution branches in the $H_0^1(\Omega)$ norm. We note from this figure that the values of $\|U_h\|_{H_0^1}$ appear to converge (to a value between 3.5 and 4) as $h \to 0$. Also away from the bifurcation point $\|U_h\|_{H_0^1}$ is roughly constant as λ is varied, although its maximum norm γ is changing. Observe that if $w_\gamma(\mathbf{x})$ is defined as in (2.9), then

$$\|w_\gamma\|_{H^1(\mathbb{R}^3)} = \frac{3^{3/4}\pi}{2} = 3.58063, \tag{5.1}$$

which is both independent of γ and close to the converged value. As the greatest contribution to the Sobolev norm of both u and of w_γ comes from the contribution due to the peak, this result is consistent with the conjecture made in section 2 that in the peak u is closely approximated by w_γ.

5.3. The form of the solution. From the calculations on the fine meshes we may draw some preliminary conclusions as to the form of the solution, in particular evidence for uniqueness, singularity, and symmetry. We summarize these here.

5.3.1. Uniqueness. An initial, simple, but important observation for the cube is that the solution branch bifurcates monotonically to the left, so that $\|U_h\|_\infty$ increases as λ decreases. In particular, there are no fold bifurcations or transcritical bifurcations on the branch and the solutions on the main branch appear to be unique for all values of $\lambda < \lambda_1$. All attempts to find additional solutions by starting from a point far distant from the main branch failed to give anything new. Accordingly, we make the conjecture that the solutions of (1.1) are *unique* in cuboid domains.

5.3.2. The behavior close to the peak. In section 2 we discussed two descriptions of the approximation, namely, approximating u^5 by a delta function and

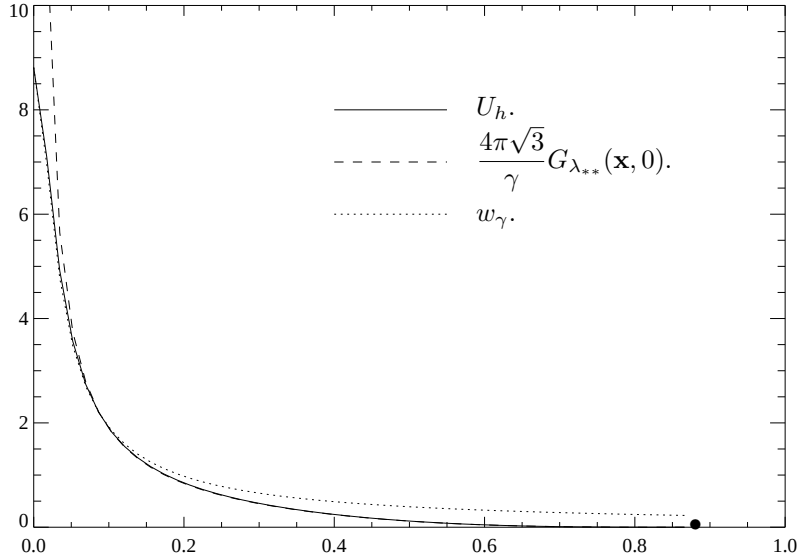

FIG. 5.5. *Graph of $U_h(\mathbf{x})$ and $w_\gamma(r)$ against $r = |\mathbf{x}|$ along the long diagonal $x = y = z$ of the cube, with $h = 1/100$, $\lambda = \lambda_{**} = 7.5045$, and $\gamma = \|U_h\|_\infty$. Also plotted is a scaling of the Green's function* (4.3) *of the linearized problem. Note that the point $r = \sqrt{3/4} = 0.866$ corresponds to a corner of the cube.*

approximating u by the function w_γ. Some support for these has already been given by the results presented in Figure 1.2. To make this comparison more precise, we take $\lambda = \lambda_{**}$, $h = 1/100$ for which we find that $\gamma \equiv \|U\|_\infty = 8.812$. In Figure 5.5 we compare U_h with w_γ. In both cases a section of the function is taken along the line $x = y = z$ with $r = \sqrt{x^2 + y^2 + z^2}$. For comparison on this graph we also plot the function $f(\mathbf{x}) \equiv 4\pi\sqrt{3}G_\lambda(\mathbf{x}, \mathbf{0})/\gamma$. (The choice of the multiplicative constant will be made clear in section 5.3.3.)

This figure is significant as it leads naturally to the asymptotic analysis that follows in section 6. Note that the approximation of U_h by w_γ is very good if $r < 0.2$, for example, $|U_h - w_\gamma|/w_\gamma < 0.15$ throughout this range, and near coincidence of the graphs as r reduces. Conversely, the approximation of U_h by f is very good if $r > 0.05$ with, again, near coincidence of the graphs. Significantly, these two ranges overlap.

In Figure 5.6 we give a section of the solution U_h with associated contours through the plane $z = 0$. This figure gives a strong indication that U_h is close to being radially symmetric for even moderately large values of $\mathbf{x}$.

To make a quantitative assessment of this symmetry and also to compare $U_h(\mathbf{x})$ with the (radially symmetric function) $w_\gamma(\mathbf{x})$ more carefully we calculate the function $e(\mathbf{x}) \equiv U_h(\mathbf{x}) - w_\gamma(\mathbf{x})$ over the same range of parameters as before, considering the three lines $l_1 \equiv \{(x, y, z) : y = z = 0\}$, $l_2 \equiv \{(x, y, z) : x = y, z = 0\}$, and $l_3 \equiv \{(x, y, z) : x = y = z\}$. The resulting three curves are then plotted in Figure 5.7. This latter graph makes it clear both that U_h is close to w_γ over a wide range and also that the function $e(\mathbf{x})$ is itself very close to being radially symmetric. Indeed, if $|\mathbf{x}| < 0.3$, then the estimates for $e(\mathbf{x})$ on the three radii differ by at most $|e(\mathbf{x})|/8$ with often better agreement. We make use of both of these observations in our asymptotic computations.

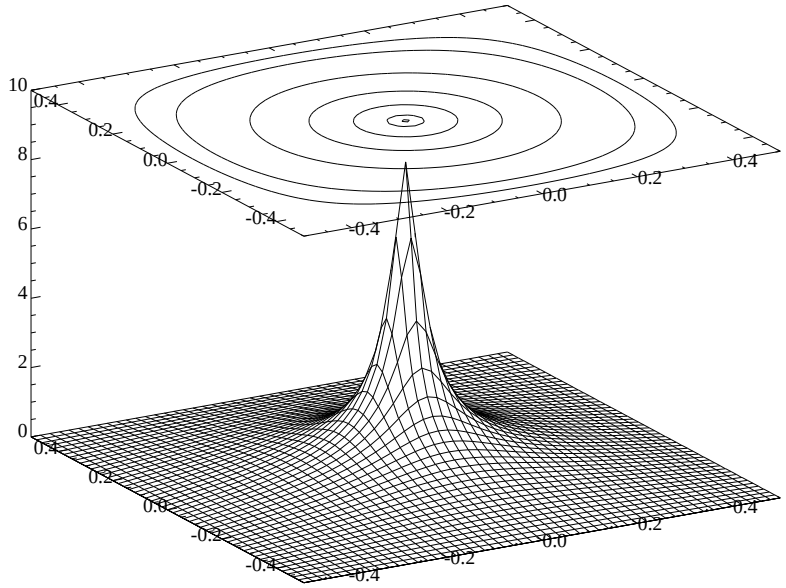

FIG. 5.6. *A cross section of U_h through center of cube with $h = 1/100$ and $\lambda = \lambda_{**} = 7.5045$, with a contour plot which clearly shows the radial symmetry of the solution in the center of the domain.*

5.3.3. Behavior away from the peak. It is clear from Figure 5.5 that away from the peak that U_h is close to $4\pi\sqrt{3}G_\lambda/\gamma$. This is consistent with the approximation for u given in (2.4) for which we had $u = AG_\lambda(\mathbf{x}, \mathbf{0})$. From section 4 we have that

$$G_\lambda(\mathbf{x}, \mathbf{0}) = \frac{1}{4\pi|\mathbf{x}|} + g_\lambda(\mathbf{x}, \mathbf{0}). \tag{5.2}$$

Now if γ is large, $\gamma^2|\mathbf{x}|$ is large, and $|\mathbf{x}|$ is small, then

$$w_\gamma(\mathbf{x}) \approx \frac{\sqrt{3}}{\gamma|\mathbf{x}|} \quad \text{and} \quad AG_\lambda(\mathbf{x}, \mathbf{0}) \approx \frac{A}{4\pi|\mathbf{x}|},$$

so the two approximate descriptions of u agree to leading order if

$$A \approx A_1 \equiv \frac{4\pi\sqrt{3}}{\gamma},$$

leading to the choice made in Figure 5.5. By making a small change to this result and taking $A = 1.012 \times 4\pi\sqrt{3}/\gamma$, then the agreement is even better, with the functions nearly coinciding. The reason for this small correction will be made evident in the next section. A comparison is made in Figure 5.8 of the difference between these two functions in this case along the three radii taken before.

From this discussion we infer the following description of U_h if γ is large.

- There is an (inner) region $|x| < r_1$ such that U_h is close to the radially symmetric function w_γ. Furthermore, the departure of U_h from radial symmetry is much smaller than the difference $|U_h - w_\gamma|$.
- There is an (outer) region $|x| > r_2$ such that u is close to AG_λ for appropriate A.

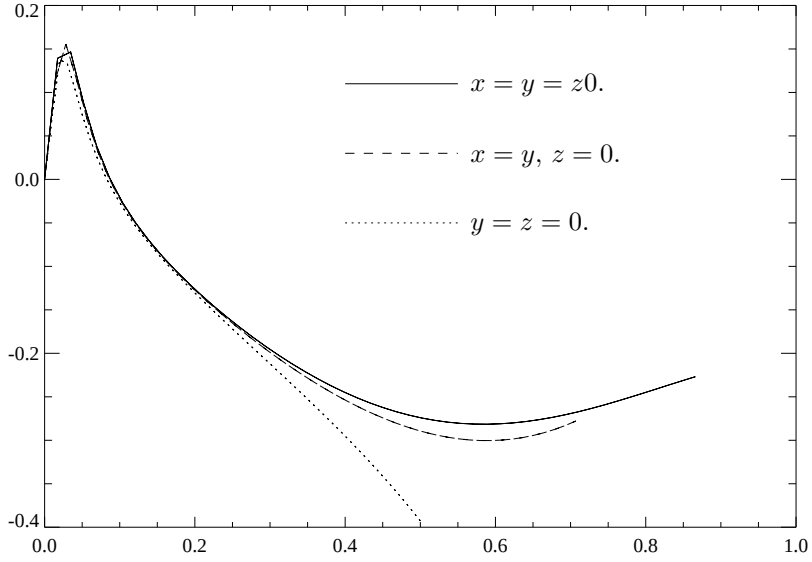

FIG. 5.7. *Graphs of* $U_h(\mathbf{x}) - w_\gamma(\mathbf{x})$ *against* $|\mathbf{x}|$ *along the three radii indicated for* $h = 1/100$ *and* $\lambda = \lambda_{**} = 7.5045$.

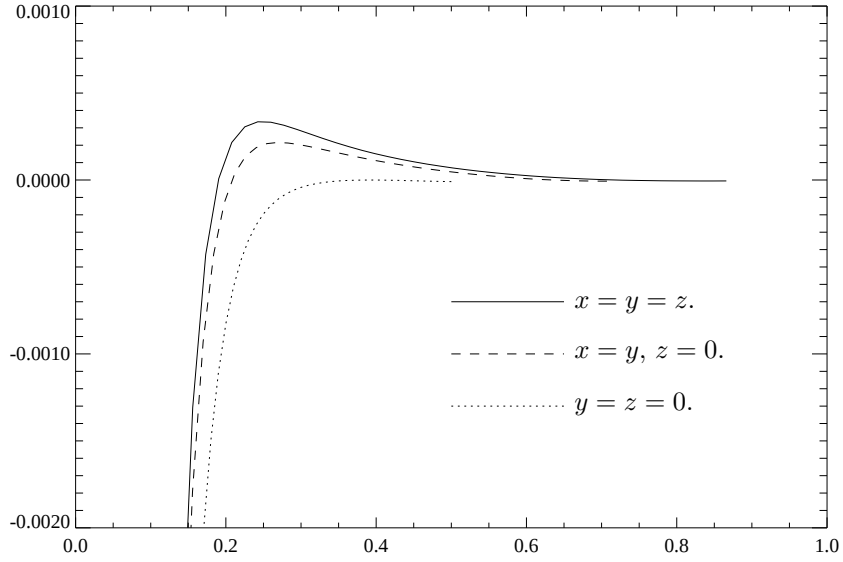

FIG. 5.8. *Graphs of* $U_h(\mathbf{x}) - 1.012\frac{4\pi\sqrt{3}}{\gamma}G_{\lambda_{**}}$ *against* $|\mathbf{x}|$ *along the same three radii indicated, with* $\gamma = \|U_h\|_\infty$, $h = 1/100$, *and* $\lambda = \lambda_{**} = 7.5045$.

Significantly, our numerical calculations strongly indicate that r_2 is somewhat less than r_1 and that both approximations are good in the annulus $r_2 < |\mathbf{x}| < r_1$. Note further that for $\lambda = \lambda_{**}$, $h = 1/100$, $\gamma = 8.812$ we can take $r_2 = 0.05$, $r_1 = 0.2$. In

the rescaled variable $\mathbf{y} = \gamma^2\mathbf{x}$ we have $\gamma^2 r_2 = 3.87$ and $\gamma^2 r_1 = 15.49$, so that, while r_1 is small, in the rescaled variables the corresponding value is relatively large. This is important for the analysis in the next section.

6. Asymptotics of the discrete solution for large γ. Motivated by the above calculations, we now develop a descriptive asymptotic theory. The results of the numerical calculations reported in the previous section have allowed us to draw some preliminary conclusions about the form of the solutions of (1.1) but are imprecise due to the relative coarseness of the discretization. To continue our discussion we now make a formal asymptotic calculation of the nature of the numerical discretization. This calculation then allows us to post-process the numerical results to obtain a more accurate picture of the form of the solution. This calculation extends those given in [15] and [5].

The principal errors in the numerical approximation occur when u is large and has a large gradient. This occurs at the peak, precisely when u is well approximated by w_γ with $\gamma = \|u\|_\infty$. Our computations have also shown that the discrete function U_h is close to w_γ if now $\gamma = \|U_h\|_\infty$. Thus we will proceed by calculating the difference between U_h and w_γ and using this calculation to estimate $\|U_h\|_\infty$. To obtain an asymptotic description of the piecewise linear function U_h we require a piecewise linear approximation of w_γ. A convenient such function is the interpolant $W_{\gamma,h}(\mathbf{x})$ to $w_\gamma(\mathbf{x})$, which is the piecewise linear function coinciding with $w_\gamma(\mathbf{x})$ on the nodes of the mesh. Provided that H is small, the functions w_γ and $W_{\gamma,h}$ are close. To do this we consider a representation of the function $U_h(\mathbf{x})$ on an inner and an outer region, such that on the *inner* region $|\mathbf{x}|$ is small and the function u is large and very close to being radially symmetric. Conversely, the outer region excludes the origin but extends to the boundary of Ω. These regions intersect in an annulus $r_1 < |\mathbf{x}| < r_2$ in which $|\mathbf{x}|$ is small but $\gamma^2|\mathbf{x}|$ is large.

6.1. The inner region. We rescale the functions so that $U_h(\mathbf{x}) = \gamma V_H(\gamma^2\mathbf{x})$, introduce the rescaled variable $\mathbf{y} = \gamma^2\mathbf{x}$, and define $W_{\gamma,h}(\mathbf{x}) = \gamma W_{1,H}(\gamma^2\mathbf{x})$, where now $W_{1,H}(\mathbf{y})$ is the piecewise linear interpolant of the function $w_1(\mathbf{y})$ on a uniform mesh of size H. Now, express the function $V_H(\mathbf{y})$ in an asymptotic series so that

$$V_H(\mathbf{y}) = V_{1,H}(\mathbf{y}) + \gamma^{-4}V_{2,H}(\mathbf{y}) + \cdots.$$

By construction, for each basis function $\varphi_i(\mathbf{x}) \in S_h$, we have the identity

$$-a(U_h, \varphi_i) + \lambda\langle U_h, \varphi_i\rangle + \langle U_h^5, \varphi_i\rangle = 0.$$

Suppose that $\varphi_{i,H}(\mathbf{y})$ is defined to be $\varphi_i(\mathbf{x})$ expressed on the rescaled mesh and that all quadratures are now calculated with respect to $\mathbf{y}$. We have

$$-a(V_H, \varphi_{i,H}) + \frac{\lambda}{\gamma^4}\langle V_H, \varphi_{i,H}\rangle + \langle V_H^5, \varphi_{i,H}\rangle = 0.$$

Substituting the asymptotic expression for V_H into the above gives equations for $V_{1,H}$, $V_{2,H}$, etc. For $V_{1,H}$ to satisfy the leading order equation exactly we would require

$$-a(V_{1,H}, \varphi_{i,H}) + \langle V_{1,H}^5, \varphi_{i,H}\rangle = 0. \tag{6.1}$$

In fact, (6.1) has the solution $w_1(\mathbf{y})$ given in (2.9), but this function is not piecewise linear. Instead we take $V_{1,H}$ to be the interpolant $W_{1,H}$ and introduce a small

discretization error into the leading order expression, which enters into the calculation of the function $V_{2,H}$. This error can be expressed in terms of a residual R_i, where

$$R_i \equiv -a(W_{1,H}, \varphi_{i,H}) + \langle W_{1,H}^5, \varphi_{i,H}\rangle.$$

Subtracting the identity (6.1) satisfied by w_1 gives

$$R_i = -a(W_{1,H} - w_1, \varphi_{i,H}) + \langle W_{1,H}^5 - w_1^5, \varphi_{i,H}\rangle. \tag{6.2}$$

Now looking at the next term in the asymptotic expansion for V_H and using (6.2) we have

$$-a(V_{2,H}, \varphi_{i,H}) + 5\langle W_{1,H}^4 V_{2,H}, \varphi_{i,H}\rangle = -\lambda\langle W_{1,H}, \varphi_{i,H}\rangle + \gamma^4 R_i. \tag{6.3}$$

As $w_1(\mathbf{y})$ is a smooth function of $\mathbf{y}$ and, for small H, the function w_1 is closely approximated by its interpolant $W_{1,H}$, we can use results from interpolation theory to estimate the magnitude of R_i. In particular we use the following result.

LEMMA 6.1. *Let $u(\mathbf{x}) \in C^4(\Omega)$ be an arbitrary function of $\mathbf{x} \in \mathbb{R}^3$, U_H its piecewise linear interpolant on a uniform mesh of size H, and $f(u)$ a differentiable function of u. Now, consider an element $\mathcal{E}$ comprising eight adjacent cubes, each of side H, centered on the origin $\mathbf{x} \equiv (x, y, z) = (0, 0, 0)$, with*

$$\varphi_H(\mathbf{x}) = \left(1 - \frac{|x|}{H}\right)\left(1 - \frac{|y|}{H}\right)\left(1 - \frac{|z|}{H}\right), \quad \mathbf{x} \in \mathcal{E}, \quad \varphi_H(\mathbf{x}) = 0 \text{ otherwise}$$

the standard basis function on this element. Then there are constants K_1 and K_2 independent of u and H, such that if H is sufficiently small, then

$$R \equiv -a(u - U_H, \varphi_H) + \big\langle f(u) - f(U_H), \varphi_H\big\rangle = H^5(A + B) + O(H^7), \tag{6.4}$$

where

$$|A| < K_1 \max_{\mathcal{E}}\big\{|u_{xxyy}| + |u_{zzyy}| + |u_{xxzz}| + |u_{xxxx}| + |u_{yyyy}| + |u_{zzzz}|\big\} \tag{6.5}$$

and

$$|B| < K_2 \max_{\mathcal{E}}\big\{|f_u(u)|(|u_{xx}| + |u_{yy}| + |u_{zz}|)\big\}. \tag{6.6}$$

Proof. Suppose first that $a_{\mathcal{E}} \equiv a(u - U_H, \varphi_H) = ax + ay + az$, where

$$ax = \int_{z=-H}^{H}\int_{y=-H}^{H}\int_{x=-H}^{H}(u_x - U_{H,x})\varphi_{H,x}\,dx\,dy\,dz, \tag{6.7}$$

with similar expressions for ay and az. Using the expression for $\varphi_H(\mathbf{x})$ and integrating (6.7) we have

$$\begin{aligned} ax &= \frac{1}{H}\int_{z=-H}^{H}\int_{y=-H}^{H}\big([u - U_H]_{-H}^{0} - [u - U_H]_{0}^{H}\big)\left(1 - \frac{|y|}{H}\right)\left(1 - \frac{|z|}{H}\right)dy\,dz \\ &= -\frac{1}{H}\int_{z=-H}^{H}\int_{y=-H}^{H}\big((u(H,y,z) - U_H(H,y,z)) - 2(u(0,y,z) - U_H(0,y,z)) \\ &\quad + (u(-H,y,z) - U_H(-H,y,z))\big)\left(1 - \frac{|y|}{H}\right)\left(1 - \frac{|z|}{H}\right)dy\,dz. \end{aligned} \tag{6.8}$$

By the uniqueness and linearity of interpolation, it follows that if u is an odd function of y or of z, then so is U_H. In the identity (6.8) the integration of all such odd functions vanishes. Thus we presume that the functions $u(H,y,z)$, etc., are even in y and z so that locally the function u has the expansion

$$u(x,y,z) = p(x) + q(x)y^2 + r(x)z^2 + s(x)y^4 + t(x)y^2z^2 + n(x)z^4 + \text{h.o.t.},$$

where

$$p(x) = u(x,0,0), \quad q(x) = \frac{1}{2}u_{yy}(x,0,0), \quad r = \frac{1}{2}u_{zz}(x,0,0)$$

and $s(x) = \frac{1}{24}u_{yyyy}(x,0,0)$, etc. Now fix $x = H$ and consider the square $0 \leqslant y, z \leqslant H$. In this square we have

$$u(H,0,0) = p(H) \quad u(H,H,0) = p(H) + q(H)H^2 + \mathcal{O}(H^4),$$

$$u(H,0,H) = p(H) + r(H)H^2 + \mathcal{O}(H^4),$$

$$u(H,H,H) = p(H) + q(H)H^2 + r(H)H^2 + \mathcal{O}(H^4),$$

where the implied constant in the order H^4 terms is bounded by a multiple of $(|u_{yyyy}| + |u_{yyzz}| + |u_{zzzz}| + \mathcal{O}(H^2))$. From these point values we can calculate U_H. This then gives

$$u(H,y,z) = p(H) + q(H)y^2 + r(H)z^2 + \mathcal{O}(H^4),$$

$$U_H(H,y,z) = p(H) + q(H)Hy + r(H)Hz + \mathcal{O}(H^4),$$

so that

$$u(H,y,z) - U_H(H,y,z) = q(H)y(y-H) + r(H)z(z-H) + \mathcal{O}(H^4).$$

Similar expressions apply when $0 \leqslant y, z \leqslant H$ and $x = 0$ or $x = -H$. Thus, over the set $0 \leqslant y, z \leqslant H$ the contribution to the integral in (6.8) is given by

$$\begin{aligned}
&-\frac{1}{2H}\int_0^H\int_0^H \Big[y(y-H)\big(u_{yy}(H,0,0) - 2u_{yy}(0,0,0) + u_{yy}(-H,0,0)\big) \\
&\qquad + z(z-H)\big(u_{zz}(H,0,0) - 2u_{zz}(0,0,0) + u_{zz}(-H,0,0)\big) \\
&\qquad + \mathcal{O}(H^4)\Big]\left(1-\frac{y}{H}\right)\left(1-\frac{z}{H}\right)dy\,dz \\
&= -\frac{1}{2H}\int_0^H\int_0^H \Big[y(y-H)\big(H^2u_{yyxx}(0,0,0) + \mathcal{O}(H^4)\big) \\
&\qquad + z(z-H)\big(H^2u_{zzxx}(0,0,0) + \mathcal{O}(H^4)\big) \\
&\qquad + \mathcal{O}(H^4)\Big]\left(1-\frac{y}{H}\right)\left(1-\frac{z}{H}\right)dy\,dz \\
&= \mathcal{O}(H^5).
\end{aligned}$$

Here the implied constant in the order term is bounded by a multiple of $(|u_{yyxx}| + |u_{zzxx}| + |u_{yyyy}| + |u_{yyzz}| + |u_{zzzz}| + \mathcal{O}(H^2))$. Repeating this argument for the different ranges of y and z and then for ay and az gives (6.5).

Now, let $b_{\mathcal{E}} = |\langle f(u) - f(U_H), \varphi_H \rangle|$. As u and U_H are close if H is small, we can estimate this by $b \leqslant \max_{\mathcal{E}}\{|f_u(u)|\}\{|u - U_H|\}\langle 1, \varphi_H \rangle$. Now, standard results from interpolation theory imply that there is a constant K independent of u such that

$$\max_{\mathcal{E}}\{|u - U_H|\} < KH^2 \max_{\mathcal{E}}\{|u_{xx}| + |u_{yy}| + |u_{zz}|\}.$$

As $\langle 1, \varphi_H \rangle < 4H^3$, this gives $b_{\mathcal{E}} < H^5 B$ with B defined in (6.6).

Combining these expressions gives the result in the lemma. □

To apply this result to calculate R_i, we take $u = w_1, f(u) = u^5$ and note that the choice of the origin as being the center of the element was quite arbitrary.

Now we consider again (6.3). For large $s = |\mathbf{y}|, w_1(\mathbf{y}) \approx \sqrt{3}/s$ so that $\langle W_{1,H}, \varphi_{i,H} \rangle = \mathcal{O}(H^3/s)$. Now the second derivatives of w_1 vary as $1/s^3$, and the fourth derivatives as $1/s^5$. Suppose that we look at the value of R_i corresponding to an element centered on $\mathbf{y}$. We can thus estimate that the corresponding values of A_i and B_i from (6.5), (6.6) to be

$$A_i < \frac{\alpha}{|\mathbf{y}|^5}, \quad B_i < \frac{\beta}{|\mathbf{y}|^7}, \tag{6.9}$$

where α and β are bounded independently of i. For this range we have $\langle W_{1,H}, \varphi_{i,H} \rangle \gg R_i$ provided that $H^3/s \gg \gamma^4 H^5/s^5$, which is satisfied if $s^4 \gg \gamma^4 H^2$, i.e., if $r \gg h$. Assuming this is the case (consistently with our numerical observations), we have that to a very good approximation

$$-a(V_{2,H}, \varphi_{i,H}) = -\left\langle \frac{\lambda\sqrt{3}}{s}, \varphi_{i,H} \right\rangle.$$

This equation is the weak form of

$$\Delta v = -\frac{\lambda\sqrt{3}}{s},$$

which has the solution

$$v(s) = \frac{a}{s} + b - \frac{\lambda\sqrt{3}}{2}s.$$

For large $\mathbf{y}$ this solution is smooth and has small second derivative terms proportional to $1/s^3$. The discrete solution is consequently a perturbation with discretization error proportional to H^2/s^3. Hence there are constants a_H, b_H such that

$$V_{2,H}(\mathbf{y}) = \left(\frac{a_H}{|\mathbf{y}|} + b_H - \frac{\lambda\sqrt{3}|\mathbf{y}|}{2}\right)\left(1 + \mathcal{O}(H^2/|s|^2)\right). \tag{6.10}$$

We use quadrature to estimate the value of the constant b_H. A direct calculation shows that the function

$$\psi(\mathbf{y}) \equiv \frac{(1 - \frac{|\mathbf{y}|^2}{3})}{(1 + \frac{|\mathbf{y}|^2}{3})^{3/2}} = \frac{\partial w_\gamma}{\partial \gamma} \quad \text{evaluated at } \gamma = 1$$

satisfies the partial differential equation

$$\Delta\psi + 5w_1^4\psi = 0.$$

Set $\Psi_H(\mathbf{y})$ to be the piecewise linear interpolant to the function $\psi(\mathbf{y})$. Differentiating (6.3) with respect to γ we have that $\forall\, i$

$$-a(\Psi_H, \varphi_{i,H}) + \langle 5W_{1,H}^4 \Psi_H, \varphi_{i,H}\rangle = \gamma^3 T_i. \tag{6.11}$$

The exact expression for T_i is complex, but simple scaling arguments imply that there exists a constant C such that $|T_i| < C|R_i|$. (See the more detailed calculation given in [5].) We now calculate b_H by using a discrete form of the divergence theorem. Consider a cube $\mathcal{C} \subset \Omega_\gamma$ aligned with the mesh, centered on the origin, and of side $2S$, where S is large and an integer multiple of H. Now introduce piecewise linear functions $\hat{\Psi}_H$ and $\hat{V}_{2,H}$ which coincide with Ψ_H and $V_{2,H}$ at all mesh points *interior* to $\mathcal{C}$, but which are zero on the boundary of, and exterior to, $\mathcal{C}$. As both the functions $\hat{\Psi}_H$, $\hat{V}_{2,H}$ are in the span of the set of functions $\varphi_{i,H}$, there exist V^i, Ψ^i such that

$$\hat{V}_{2,H} = \sum V^i \varphi_{i,H}, \quad \hat{\Psi}_H = \sum \Psi^i \varphi_{i,H}.$$

Taking a linear combination of (6.3) and (6.11) and subtracting give

$$\begin{aligned} &-a(V_{2,H}, \hat{\Psi}_H) + \langle 5W_{1,H}^4 V_{2,H}, \hat{\Psi}_H\rangle + a(\Psi_H, \hat{V}_{2,H}) - \langle 5W_{1,H}^4 \Psi_H, \hat{V}_{2,H}\rangle \\ &\qquad = -\lambda\langle W_{1,H}, \hat{\Psi}\rangle + \gamma^4 \sum \Psi^i R_i(\mathbf{y}) - \gamma^3 \sum V^i T_i(\mathbf{y}). \end{aligned} \tag{6.12}$$

The left-hand side of (6.12) has two contributions given by

$$a(\Psi_H, \hat{V}_{2,H}) - a(V_{2,H}, \hat{\Psi}_H) \equiv a(\Psi_H - \hat{\Psi}_H, V_{2,H}) - a(V_{2,H} - \hat{V}_{2,H}, \Psi_H) \tag{6.13}$$

and

$$\begin{aligned} &5\big(\langle W_{1,H}^4 V_{2,H}, \hat{\Psi}_H\rangle - \langle W_{1,H}^4 \Psi_H, \hat{V}_{2,H}\rangle\big) \\ &\qquad \equiv 5\big(\langle W_{1,H}^4 (\Psi_H - \hat{\Psi}_H), V_{2,H}\rangle - \langle W_{1,H}^4 (V_{2,H} - \hat{V}_{2,H}), \Psi_H\rangle\big). \end{aligned} \tag{6.14}$$

Both of these expressions have contributions only from integrals over those cubes adjacent to the boundary of $\mathcal{C}$. Furthermore, for large $\mathbf{y}$ the terms in expression (6.13) completely dominate those in (6.14) and we need only consider their contribution to (6.12). Consider (6.13), first taking the expression

$$a(\Psi_H - \hat{\Psi}_H, V_{2,H}). \tag{6.15}$$

Now set $\chi = \Psi_H - \hat{\Psi}_H$ and $t = V_{2,H}$. Then if $-S < y, z < S$, we have $\chi(S-H, y, z) = 0$ and $\chi(S, y, z) = \Psi_H(S, y, z)$. Now consider the face of $\mathcal{C}$ for which $x = S$ is constant. The contribution to (6.15) from integrals over cubes adjacent to this face is

$$\int_{y=-S}^{S}\int_{z=-S}^{S}\int_{x=S-H}^{S} (\chi_x t_x + \chi_y t_y + \chi_z t_z)\, dx\, dy\, dz.$$

As χ and t are piecewise linear functions, it follows that $\chi_x t_x$ does not depend upon x. Thus

$$\int_{x=S-H}^{S} \chi_x t_x\, dx = \Psi_H(S, y, z)(V_{2,H})_x(S, y, z), \tag{6.16}$$

where the derivative of $V_{2,H}$ is the value attained as x tends to S from below. Similarly, a direct calculation gives

$$\begin{aligned}(6.17)\qquad &\int_{x=S-H}^{S} \chi_y t_y \, dy\, dz \\ &\quad = \frac{H}{6}(\Psi_H)_y(S,y,z)\big(2(V_{2,H})_y(S,y,z) + (V_{2,H})_y(S-H,y,z)\big),\end{aligned}$$

with a similar result for $\chi_z t_z$. If we now consider the contribution over the same face of $\mathcal{C}$ of the second term $a(V_{2,H} - \hat{V}_{2,H}, \Psi_H)$ in (6.13) we obtain identical expressions to (6.16), (6.17) but with $V_{2\,H}$ and Ψ_H interchanged. Subtracting the two expressions of the form (6.17) gives

$$\begin{aligned}&\frac{H}{6}\big[((\Psi_H)_y(S-H,y,z)(V_{2,H})_y(S,y,z)) - (\Psi_H)_y(S,y,z)(V_{2,H})_y(S-H,y,z)\big] \\ &\qquad = \mathcal{O}(H^2).\end{aligned}$$

Repeating this calculation over the faces $y = S$ and $z = S$ and combining these results give

$$\begin{aligned}(6.18)\qquad &a(\Psi_H - \hat{\Psi}_H, V_{2,H}) - a(V_{2,H} - \hat{V}_{2,H}, \Psi_H) \\ &\qquad = \int_{\partial\mathcal{C}} \big(\Psi_H \nabla V_{2,H} - V_{2,H}\nabla\Psi_H\big).\mathbf{dA} + \mathcal{O}(H^2),\end{aligned}$$

where $\mathbf{dA}$ is the surface area element of the cube with outward pointing normal, and the gradients are taken in an inner neighborhood of the boundary. The contribution to (6.18) by the term involving the constant b_H is given by

$$\int_{\partial\mathcal{C}} b_H \nabla\Psi_H.\mathbf{dA}.$$

From the explicit form of ψ we have for large $\mathbf{y}$ that $\nabla\Psi_H = \nabla\psi + \mathcal{O}(H/|\mathbf{y}|^3)$ and hence, evaluating the integral of $\nabla\psi$ over the cube explicitly, we have

$$\int_{\partial\mathcal{C}} b_H \nabla\Psi_H.\mathbf{dA} = 4\pi\sqrt{3}b_H\left(1 + \mathcal{O}\left(\frac{1}{|\mathbf{y}|^2}\right) + \mathcal{O}\left(\frac{H}{|\mathbf{y}|}\right)\right).$$

The other principal contribution to (6.18) is then given by the surface integral of $-3\lambda\mathbf{y}/|\mathbf{y}|^2$ which evaluates explicitly to αS, where

$$\alpha = -18\lambda\int_{-1}^{1} \frac{\arctan(\frac{1}{\sqrt{1+t^2}})}{\sqrt{1+t^2}}dt.$$

Returning to expression (6.12) we then have, to leading order,

$$4\pi\sqrt{3}b_H\left(1 + \mathcal{O}\left(\frac{1}{|\mathbf{y}|^2}\right) + \mathcal{O}\left(\frac{H}{|\mathbf{y}|}\right)\right) + \alpha S = \sum \gamma^4 \Psi_H^i R_i - \gamma^3 V^i T_i - \langle \lambda W_{1,H}, \hat{\Psi}_H\rangle.$$

In the above, the inner product $\langle \lambda W_{1,H}, \hat{\Psi}_H\rangle$ is the discrete form of the integral $\langle w_1, \psi\rangle$ over the cube. Again, this can be evaluated explicitly and for large S converges to $(\alpha S + 12\pi\sqrt{3}\pi\lambda)(1 + \mathcal{O}(H^2))$. Here, the constant implied in the $\mathcal{O}(H^2)$ term does not involve γ. Now consider the two sums which are taken over the elements interior

to $\mathcal{C}$. As R_i decays rapidly for large $|\mathbf{y}|$, both sums rapidly tend toward a finite limit as S increases; thus we may take the sums to be infinite. This sum may be evaluated numerically by using the explicit construction for R_i over successively larger cubes and finer meshes. Note that as R_i and T_i scale as H^5 and the cube $\mathcal{C}$ contains $8S^3/H^3$ cubes of side H, the resulting sums scale as H^2. Numerical experiments confirm this relation. By making a series of calculations over successively finer meshes and for cubes of increasing size we estimate that

$$\sum_{i=1}^{\infty} \gamma^4 \Psi_H^i R_i = -0.383184 H^2 \gamma^4 + \mathcal{O}(H^3).$$

Now the terms T_i each have similar magnitude to the terms R_i. Consequently, estimating $V_{2,H}$ by the dominant contribution of s we have that the sum involving T_i is, at worst, of order H^2, where the implied constant does not depend upon γ and this sum is thus dominated by the terms involving R_i.

By comparing constant terms in the expression for b_H we then have

$$b_H = -0.017605 H^2 \gamma^4 + 3\pi\lambda + \mathcal{O}(H^2). \tag{6.19}$$

We note that this estimate for b_H does *not* depend upon the domain, but does depend upon the fact that we are using cubes as elements. In principle we can also calculate b_H for other element shapes. (In [5] a similar calculation of b_H for elements comprising concentric circles gave

$$b_H = -0.008863 H^2 \gamma^4 + 3\pi\lambda + \mathcal{O}(H^2).)$$

Combining our estimates and rescaling we can derive an inner expression for U_H for r small and s large of the form

$$U_h = \gamma W_{1,H}(\gamma^2 x) + \gamma^{-3}\left(\frac{a}{\gamma^2|r|} + b_H - \frac{\lambda\sqrt{3}}{2}\gamma^2 r\right) \tag{6.20}$$

with b_H given by (6.19).

6.2. The outer region. The analysis in the outer region is much simpler as here the solution u is smooth and $U_h(\mathbf{x})$ is a good approximation. The error made in this approximation is proportional to $h^2 u''$ and does not involve γ. In this region we have (from the discussion in section 5) that

$$u(\mathbf{x}) \approx \frac{4\pi\sqrt{3} G_\lambda(\mathbf{x}, 0)}{\gamma} = \frac{\sqrt{3}}{\gamma}\left(\frac{1}{r} + 4\pi g_\lambda(\mathbf{x}, \mathbf{0})\right).$$

In [5] it is shown that

$$g_\lambda(\mathbf{x}, 0) = g_\lambda(0, 0) - \frac{\lambda}{8\pi} r + \mathcal{O}(r^2);$$

hence, we predict that as r is reduced

$$U_h(\mathbf{x}) = \frac{\sqrt{3}}{\gamma}\left(\frac{1}{r} + 4\pi g_\lambda(0,0) - \frac{\lambda}{2} r\right)\left(1 + \mathcal{O}\left(\frac{h^2}{r^2}\right)\right), \tag{6.21}$$

where the error is small provided that $r \gg h$. A more complete analysis of the error made in this expression for the closely related radially symmetric problem term is given in [5].

6.3. Matching. The two expressions (6.20) and (6.21) can be compared in a region where r and u are small and s is large. Expanding (6.20) gives

$$U_h = \frac{\sqrt{3}}{\gamma r} + \frac{b_H}{\gamma^3} + \frac{a_H}{\gamma^5 r} - \frac{\lambda\sqrt{3}}{2\gamma} r - \frac{\lambda\sqrt{3} r}{2\gamma}.$$

Comparing with (6.21) we have excellent agreement provided that

$$\frac{b_H}{\gamma^3} = \frac{4\pi\sqrt{3} g_\lambda(\mathbf{0},\mathbf{0})}{\gamma}.$$

Substituting (6.19) into this relation and rescaling give in the limit of large γ

$$\frac{-0.017605}{3\pi\lambda} h^2\gamma^6 + \gamma^{-2} = \frac{4}{\sqrt{3}\lambda} g_\lambda(\mathbf{0},\mathbf{0}) + \mathcal{O}\left(\frac{1}{\gamma^4}\right) \tag{6.22}$$

for those values of h for which $H \ll 1$. The expression (6.22) gives an asymptotic description of the value of $\|U_h\|_\infty$. Significantly, (6.22) is satisfied by a *finite* value of γ when $g_\lambda(0,0) = 0$.

(Note further that even better agreement is obtained if the multiplying factor of $4\pi\sqrt{3}/\gamma$ is replaced by $4\pi\sqrt{3}/\gamma(1+a_H/\sqrt{3}\gamma^4)$, which accounts for the small correction noted in section 5.)

7. Conclusions from the asymptotic formulae. In this final section we now look at the predictions of the formula (6.22). We show that they are fully consistent with the numerical calculations. This gives support to the validity of the approach and also allows us to extrapolate the results to obtain a more accurate picture of the solution. These results can then be used as the basis of error estimates both for an adaptive mesh procedure and for calculations on other domains; see [6].

7.1. Divergence for $\boldsymbol{\lambda = \lambda_{**}}$. For $\lambda \leqslant \lambda_{**}$ we have $g_\lambda(\mathbf{0},\mathbf{0}) \leqslant 0$. It is possible for the expression (6.22) to have solutions in this case, and these grow as h is reduced. This is fully consistent with the prediction of the existence of the spurious solutions. In particular, if we set $\lambda = \lambda_{**}$ so that $g_\lambda(\mathbf{0},\mathbf{0}) = 0$, then for (6.22) to apply we must have

$$\gamma = \left(\frac{3\pi\lambda_{**}}{0.017605}\right)^{1/8} h^{-1/4} = 2.821 h^{-1/4}, \tag{7.1}$$

giving (1.7). This result is in excellent agreement with the results presented in Table 5.2. The agreement is especially good when we consider that the calculated value of H when $h = 1/100$ is 0.774, which is not particularly small.

When $\lambda < \lambda_{**}$ the asymptotic formula predicts that γ grows like $h^{-1/4}$ for moderate values of γ and like $h^{-1/3}$ for larger values. Numerical experiments can be made only on feasible meshes for the moderate values, and $\mathcal{O}(h^{-1/4})$ rates of growth are indeed observed in these cases.

7.2. Convergence for $\boldsymbol{\lambda > \lambda_{**}}$. If we substitute $h = 0$ into (6.22) we get an approximation Γ for $\|U_h\|_\infty$ such that

$$\frac{-0.017605}{3\pi\lambda} h^2\gamma^6 + \gamma^{-2} \approx \Gamma^{-2} \tag{7.2}$$

so that

$$\Gamma \approx \gamma/\sqrt{1 - Ch^2\gamma^8/\lambda}, \tag{7.3}$$

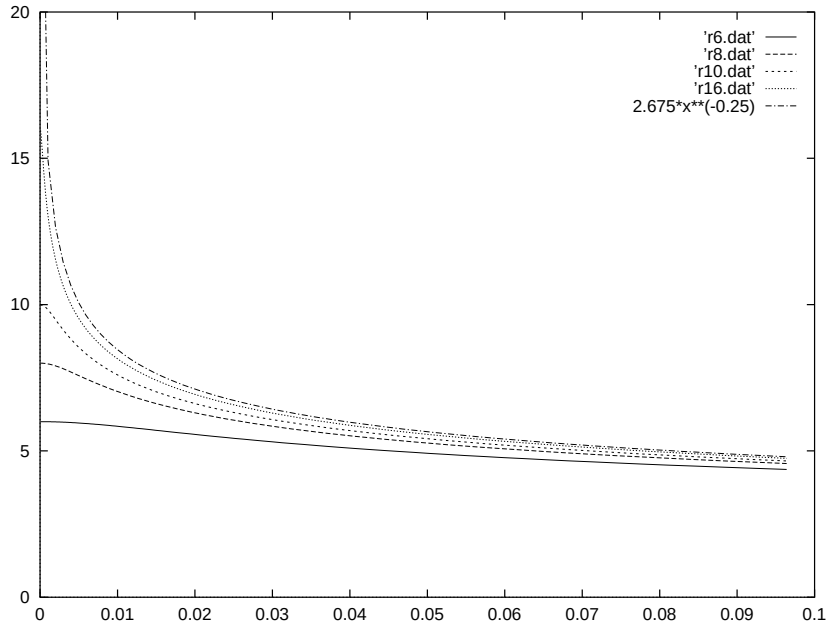

FIG. 7.1. *The value of* $\|U_h\|_\infty$ *as a function of* h *in the cases of* $\|u\|_\infty = 6, 8, 10, 16, \infty$.

where $C = 0.0018679$ giving (1.6) in the introduction. In the limit of very small h we have

$$\frac{\Gamma - \gamma}{\gamma} = \frac{C\gamma^8 h^2}{2\lambda}, \tag{7.4}$$

giving the result (1.5) in the introduction.

Observe that h has to be taken sufficiently small so that $h\gamma^4$ is small before the (standard) error estimate (7.4) is sharp. In fact the estimate (7.3) is descriptive over the wider range of values of h given by $h\gamma^2$ small. For values of h such that $h\gamma^2$ is small but $h\gamma^4$ is not small, the formula predicts that γ should again grow like $h^{-1/4}$ consistent with the results presented in Figure 5.3. It is of interest to compare the predictions of (7.3) with the results in Figure 5.3. Accordingly, we set $\lambda = \lambda_{**}$, take a sequence of values of $\Gamma = 6, 8, 10, 16, \infty$ (where the latter case is equivalent to using the formula (7.1)), and calculate γ as a function of h as h is reduced. This calculation gives the graph presented in Figure 7.1, which is directly comparable with Figure 5.3, and shows close similarity to it, provided that h is sufficiently small.

To compare (7.3) more precisely with the calculated values, we consider the formula

$$\Gamma = \frac{\gamma}{\sqrt{1 - Ch^2\gamma^8/\lambda}}$$

to be exact for calculations on the two successive meshes given by $h = 1/90$ and $h = 1/100$ and use this to estimate C. The resulting estimates of C when λ is close to λ_{**} are given in Table 7.1.

These values are again in good agreement with the asymptotic formula—especially that given when $\lambda = 8$.

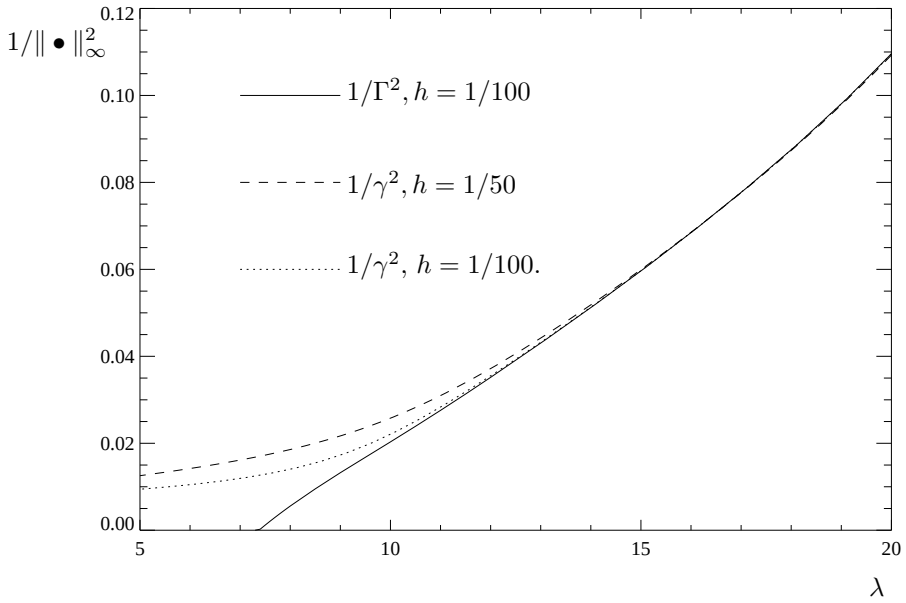

FIG. 7.2. *Graphs of* $1/\|U_h\|_\infty^2$ *for* $h = 1/50$, $1/100$ *together with the extrapolated value* $1/\Gamma^2$ *for* $h = 1/100$ *plotted against* λ.

TABLE 7.1
Estimates for C.

λ	C
7.5045	0.001531
8	0.001847
8.5	0.002168
9	0.002471
9.5	0.002783

As a final calculation, we now use (7.3) to post-process the results. For a calculated value of γ on a mesh with $h = 1/100$ we determine the value of Γ given by (7.3). This extrapolated value serves as a better estimate for $\|u\|_\infty$ than γ. In Figure 7.2 we plot the resulting value of $1/\Gamma^2$ as a function of λ compared with the value of γ obtained when $h = 1/100$ and also when $h = 1/50$.

We now see that the graph of $1/\Gamma^2$ is very close to being a straight line over a wide range of values of λ with an intercept very close to λ_{**}. This gives us further confidence in saying that $\lambda_0 = \lambda_{**}$.

The results from this discussion indicate how we should proceed to calculate on more complex domains and with finer meshes. First, the result (7.3) involves a constant which depends upon the fact that we are using cubic elements but not on the precise domain used for the integration. Thus it can be used to post-process calculations on more complex domains. Second, the result (7.4) gives an asymptotic error estimate which can be incorporated into an adaptive mesh strategy. Some preliminary indications of the effectiveness of this are given in [6].

REFERENCES

[1] H. BREZIS, *Elliptic equations with limiting Sobolev exponents—the impact of topology*, Comm. Pure Appl. Math., 39 (1986), pp. S17–S39.

[2] H. Brezis and L. Nirenberg, *Positive solutions of nonlinear elliptic equations involving critical Sobolev exponents*, Comm. Pure Appl. Math., 36 (1983), pp. 437–477.
[3] H. Brezis and L. Peletier, *Asymptotics for elliptic equations involving critical growth*, in Partial Differential Equations and the Calculus of Variations, Volume I, Birkhäuser, Boston, 1989, pp. 149–192.
[4] C. Budd, *Semilinear elliptic equations with near critical growth rates*, Proc. Roy. Soc. Edinburgh, Sect. A, 107 (1987), pp. 249–270.
[5] C. Budd and A. Humphries, *Weak finite dimensional approximations of radial solutions of semi-linear elliptic PDEs with near critical exponents*, J. Asymptotic Anal., 17 (1998), pp. 185–220.
[6] C. Budd and A. Humphries, *Adaptive methods for semilinear elliptic equations with critical exponents and interior singularities*, Appl. Numer. Math., 26 (1998), pp. 227–240.
[7] S. Chow and J. Hale, *Methods of Bifurcation Theory*, Springer-Verlag, New York, 1982.
[8] M. Crouzeix and J. Rappaz, *On Numerical Approximation in Bifurcation Theory*, Springer-Verlag, New York, 1989.
[9] M. Dobrowolski and R. Rannacher, *Finite element methods for nonlinear elliptic systems of second order*, Math. Nachr., 94 (1980), pp. 155–172.
[10] W.-M. Gidas, B. Ni, and L. Nirenberg, *Symmetry and related properties via the maximum principle*, Comm. Math. Phys., 68 (1979), pp. 209–243.
[11] P. Lions, *On the existence of positive solutions of semilinear elliptic equations*, SIAM Rev., 24 (1982), pp. 441–467.
[12] J. Lopez-Marcos and J. Sanz-Serna, *Stability and convergence in numerical analysis* iii*: Linear investigation of nonlinear stability*, IMA J. Numer. Anal., 8 (1986), pp. 71–84.
[13] B. McLeod, *A Nonlinear Elliptic Equation with Critical Sobolev Exponent*, unpublished work, 1984.
[14] F. Merle, L. Peletier, and J. Serrin, *A bifurcation problem at a singular limit*, Indiana Univ. Math. J., 43 (1994), pp. 585–609.
[15] T. Murdoch and C. Budd, *Convergent and spurious solutions of nonlinear elliptic equations*, IMA J. Numer. Anal., 12 (1992), pp. 365–386.
[16] R. Schoen, *Conformal deformation of a Riemannian metric to constant scalar curvature*, J. Differential Geom., 20 (1984), pp. 479–495.